

Solar Illumination Dependence of the Auroral Electrojet Intensity: Interplay between the Solar Zenith Angle and Dipole Tilt

S. Ohtani¹, J. W. Gjerloev^{1,2}, M. G. Johnsen³, M. Yamauchi⁴, U. Brändström⁴, and A. M. Lewis⁵

1: The Johns Hopkins University Applied Physics Laboratory, Laurel, Maryland, USA.

2: Faculty for physics and technology, University of Bergen, Bergen, Norway.

3: Tromsø Geophysical Observatory, UiT the Arctic University of Norway, Norway.

4: Swedish Institute of Space Physics, Kiruna, Sweden.

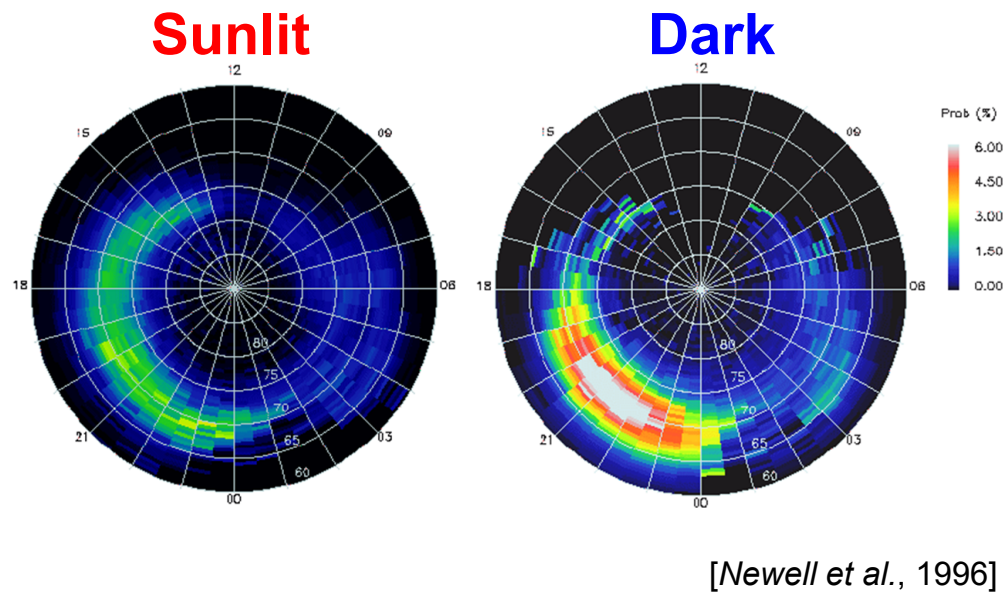
5: Geoscience Australia, Australia.

Acknowledgments:

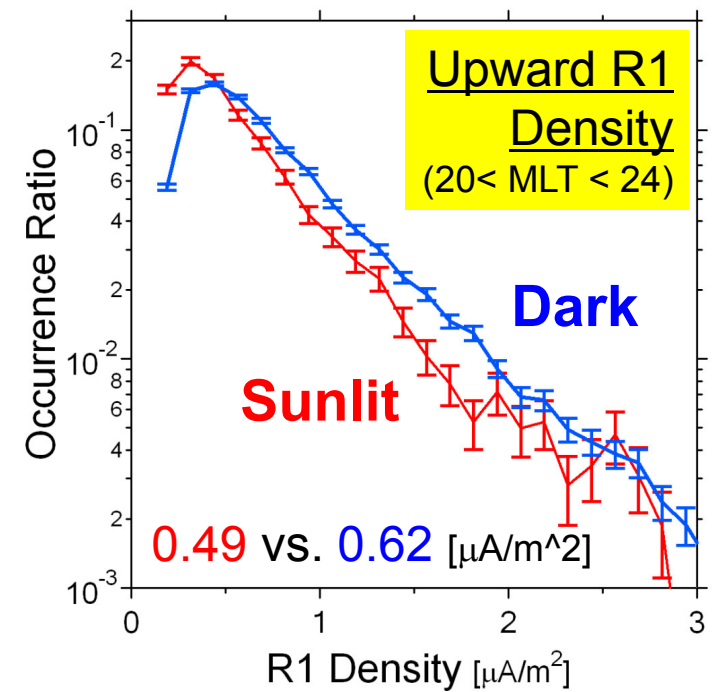
We thank the United States Geological Survey (USGS) for the College (CMO) ground magnetometer data. We also thank Sodankylä Geophysical Observatory of the University of Oulu for the Sodankylä (SOD) ground magnetometer data. The ground magnetometer data that we used in this study, including the CMO and SOD data, were provided through the SuperMAG website (<http://supermag.jhuapl.edu/>). SuperMAG is an international collaboration with many organizations and institutes funded by National Science Foundation (NSF). The OMNI data were provided by the GSFC/SPDF OMNIWeb at <https://omniweb.gsfc.nasa.gov>. Support for this analysis at the Johns Hopkins University Applied Physics Laboratory was provided by National Aeronautics and Space Administration (NASA) grant NNX16AG74G and National Science Foundation (NSF) grants 1502700 for SO, by NSF grant 1417899 for JWG.

Sunlit vs. Dark Hemispheres

e- Precipitation

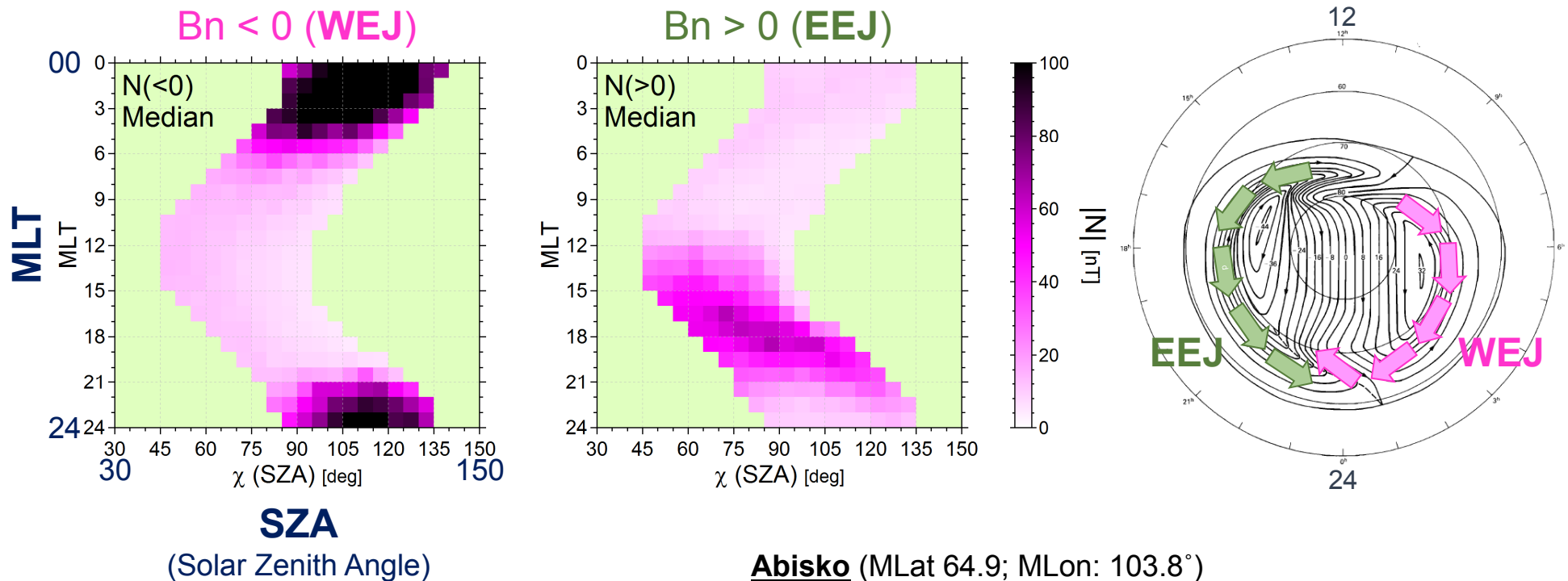


Upward R1



Westward Electrojet (WEJ) & Eastward Electrojet (EEJ)

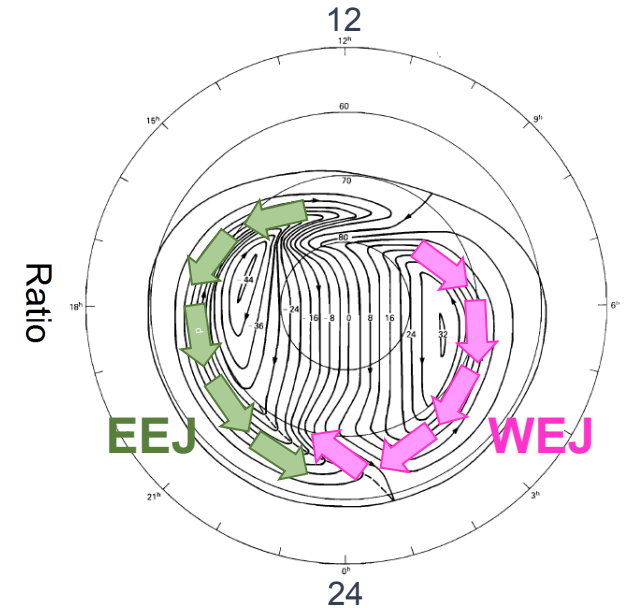
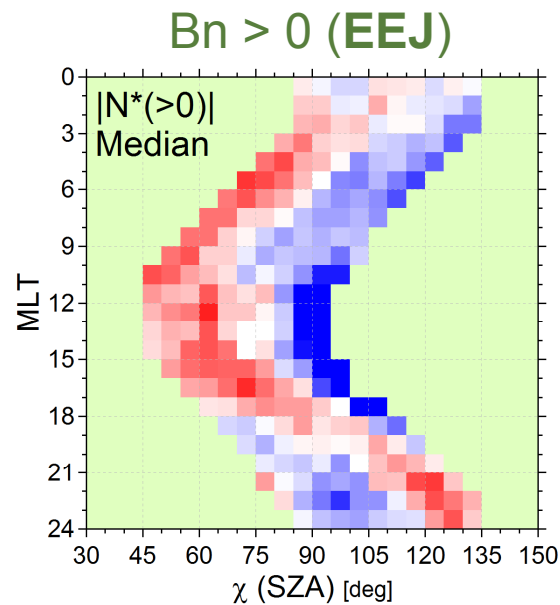
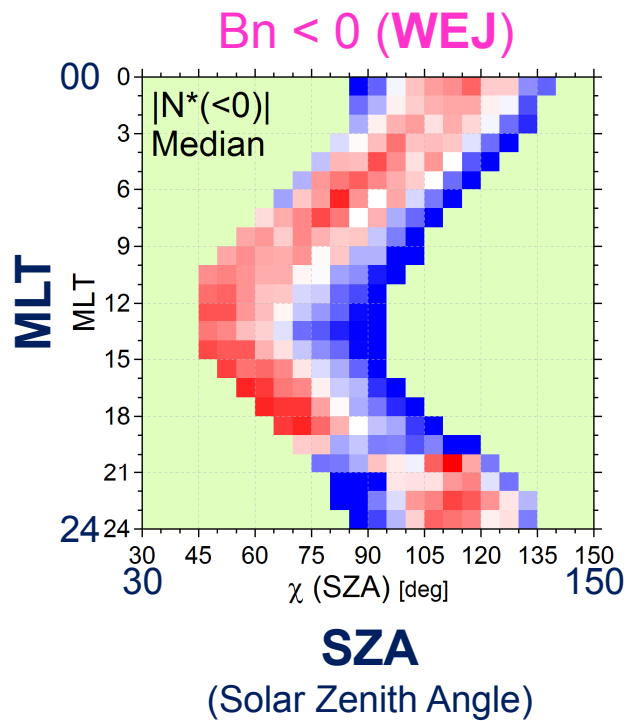
Bn: Northward component provided by SuperMAG, practically the same as H



- 5-min averages of perturbations for 1979~2017 (38 years)
- $|B_N| > |B_Z|$

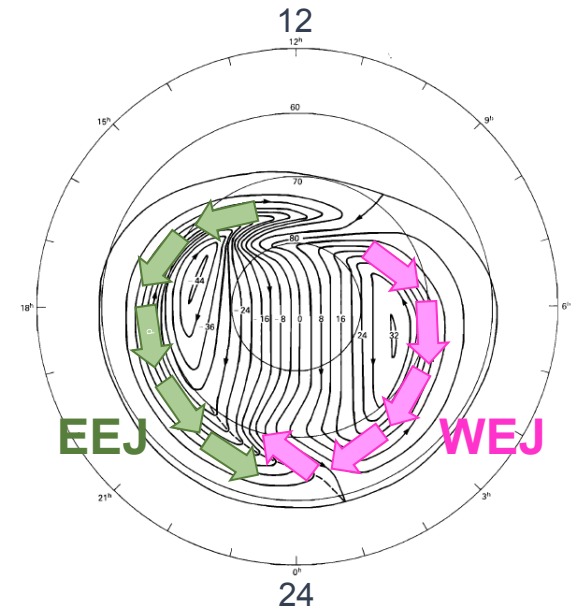
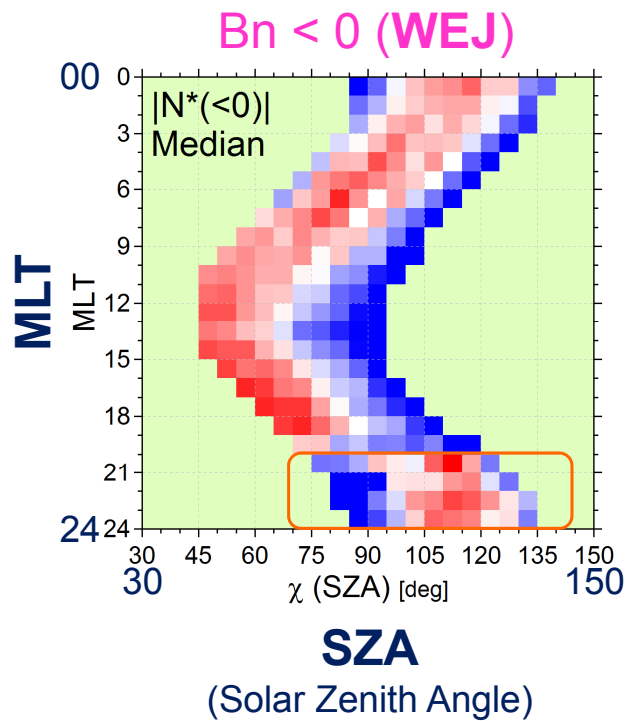
Westward Electrojet (WEJ) & Eastward Electrojet (EEJ)

red/blue: larger/smaller than average

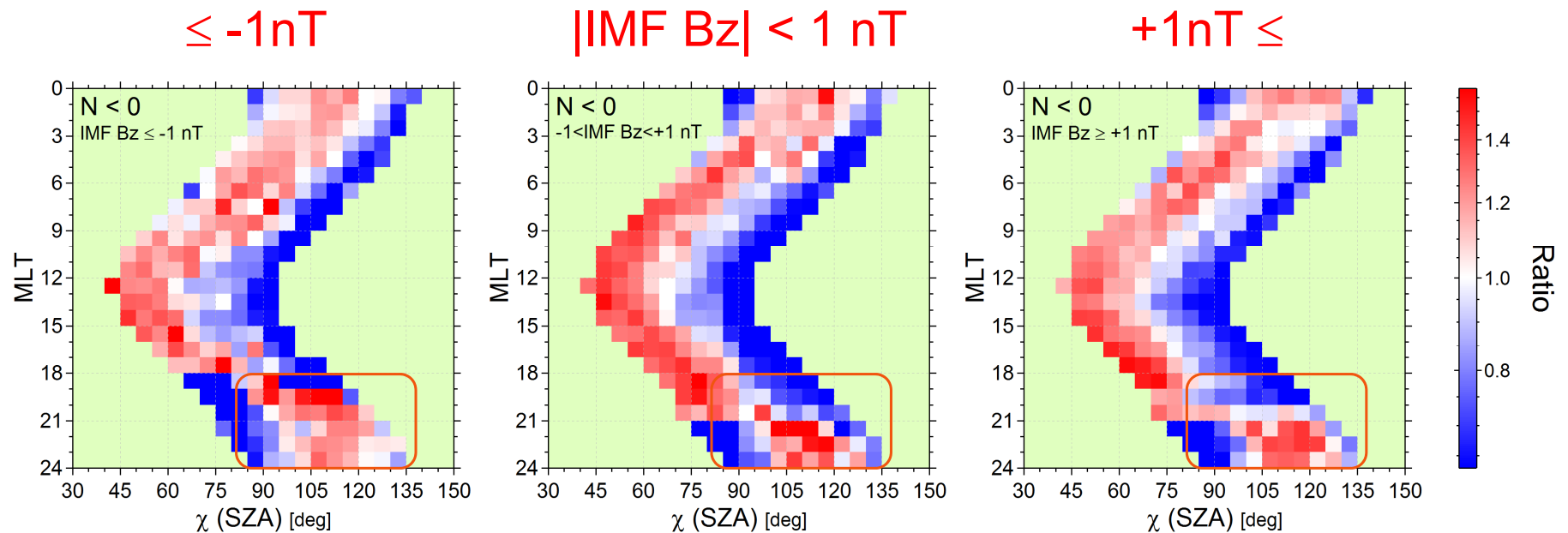


Westward Electrojet (WEJ) & Eastward Electrojet (EEJ)

red/blue: larger/smaller than average

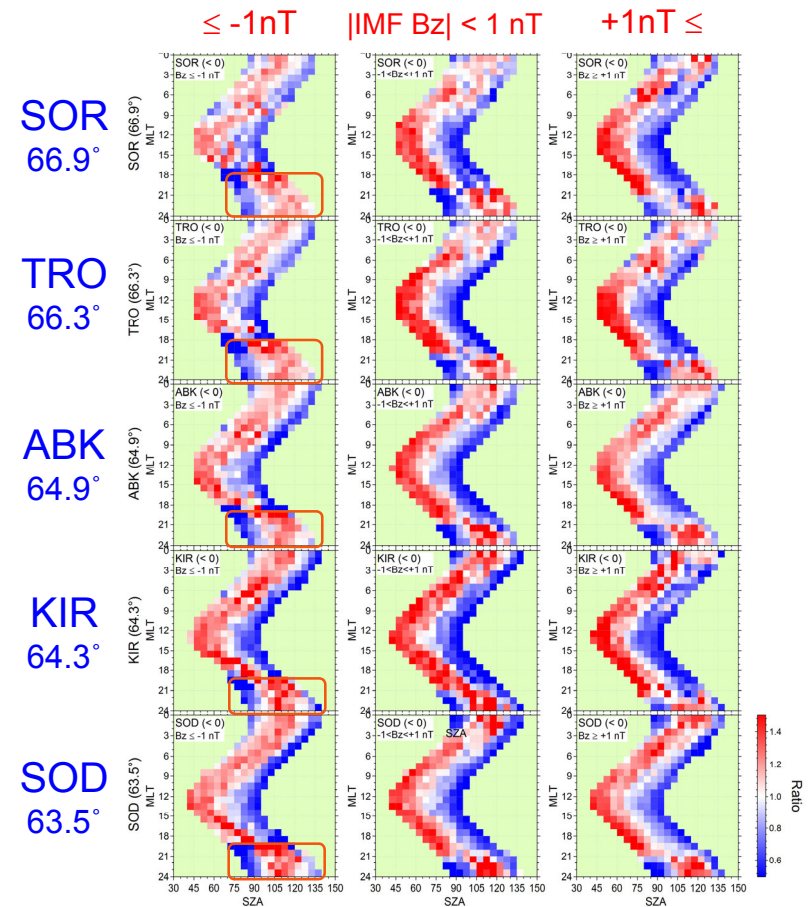
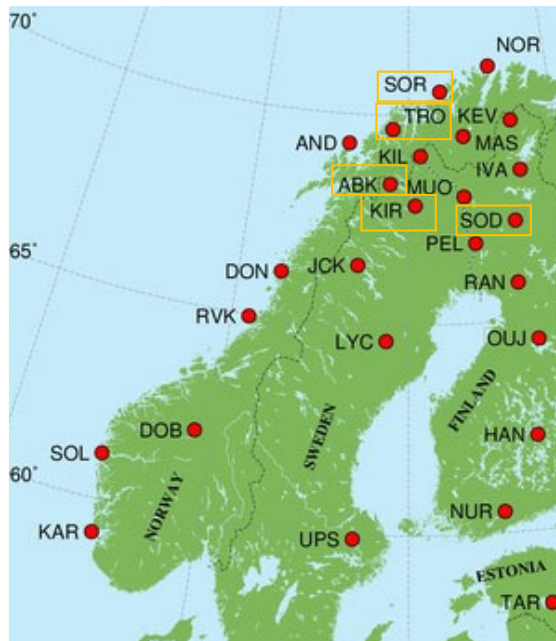


Blue-to-red pattern extends duskward for IMF Bz < 0

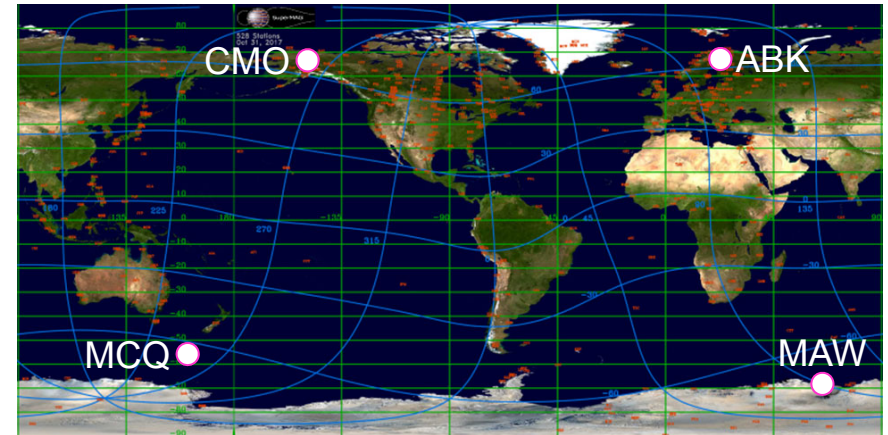
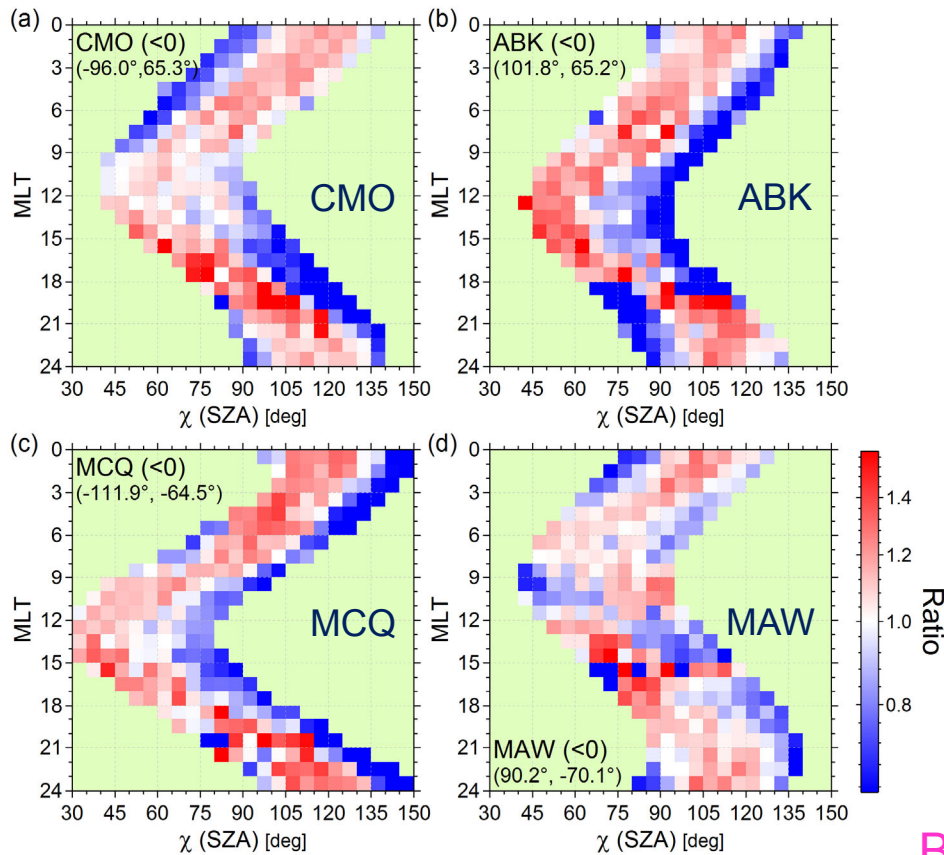


IMF Bz: -60 to -5 min OMNI data average before each 5-min data point

Consistent blue-to-red pattern in the auroral zone



Patterns are not consistent among four stations!?



College (CMO)
(-98.2°, 64.9°)

Abisko (ABK)
(103.8°, 64.9°)

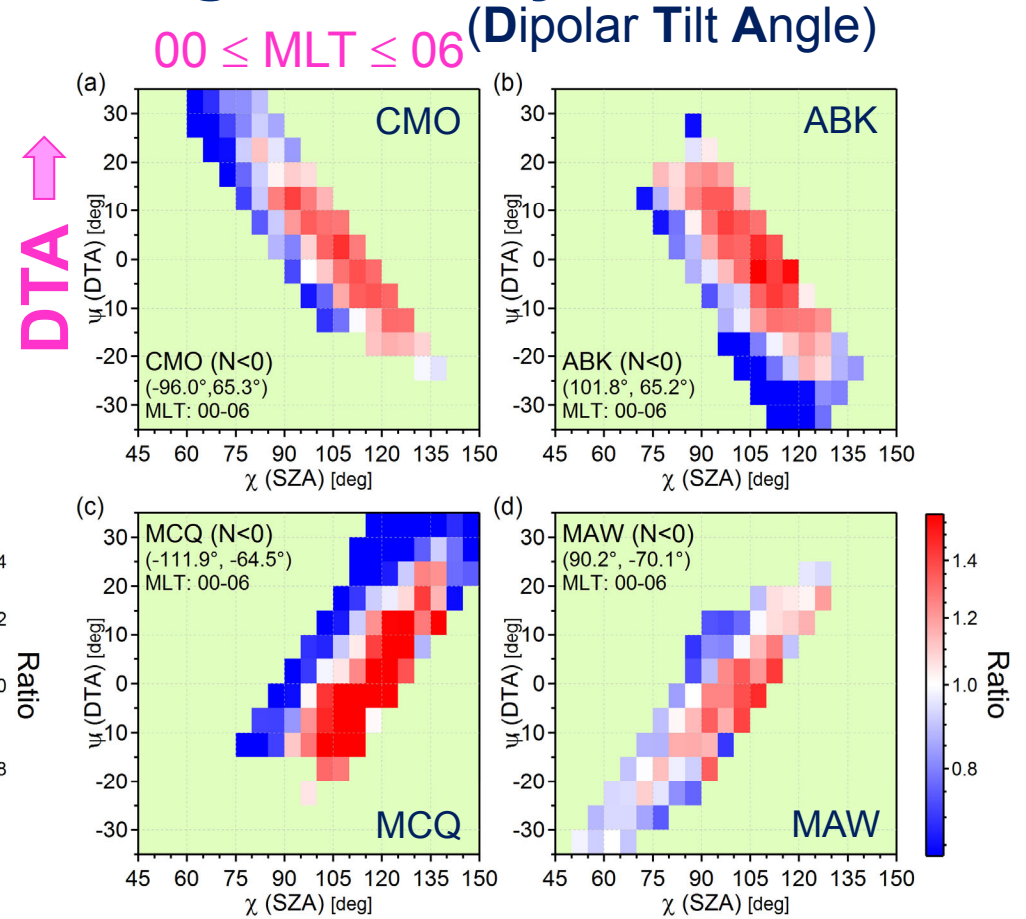
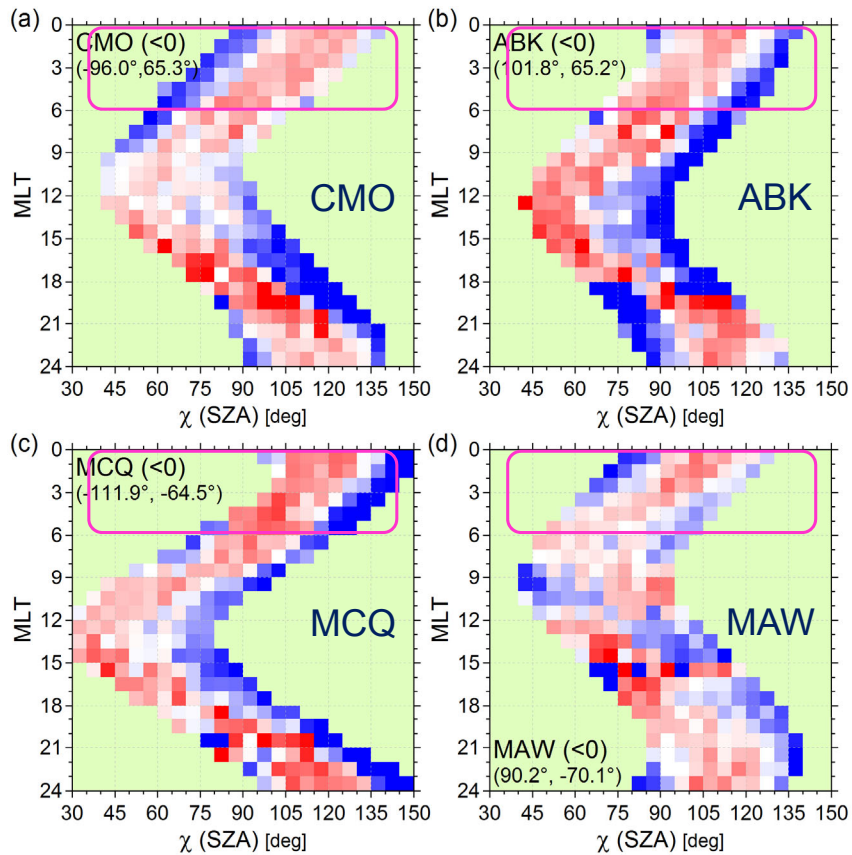
Macquarie Is. (MCQ)
(-112.0°, -64.6°)

Mawson (MAW)
(89.9°, -70.1°)

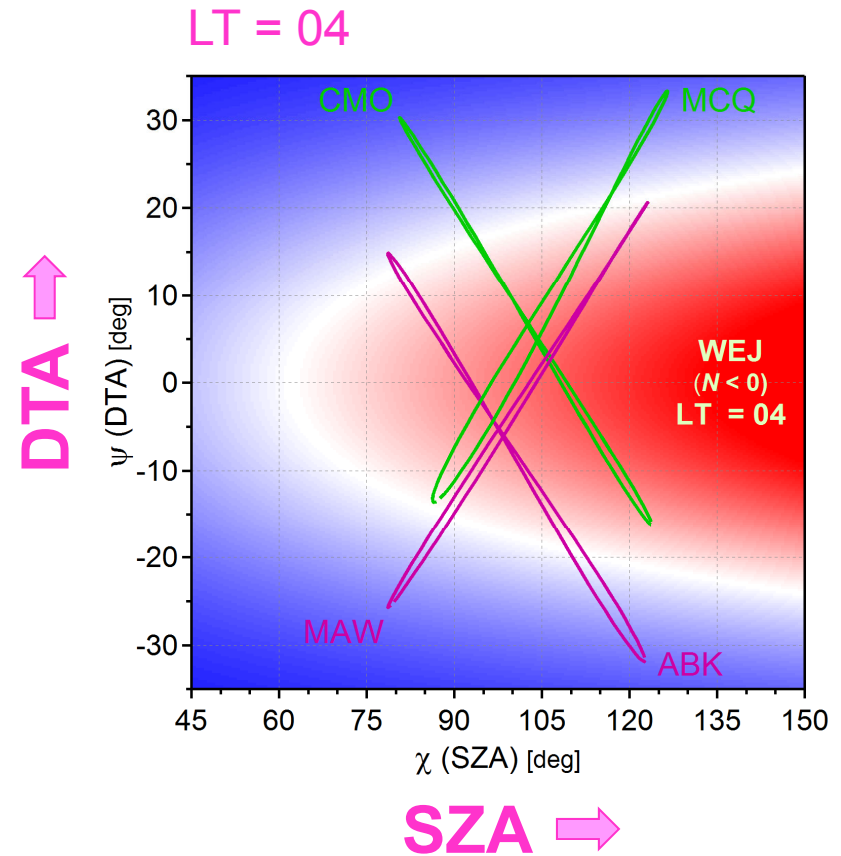
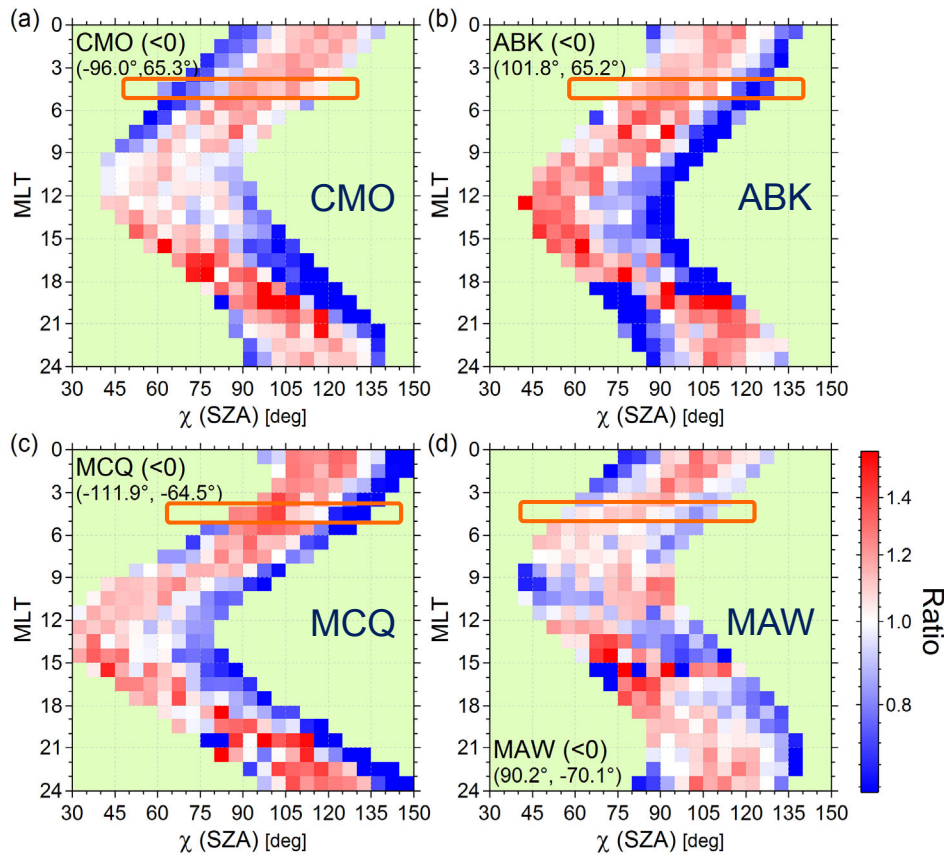
$B_n < 0$ (WEJ) for IMF $B_z \leq -1\text{nT}$

Consistency emerges once organized by DTA!

(Dipolar Tilt Angle)

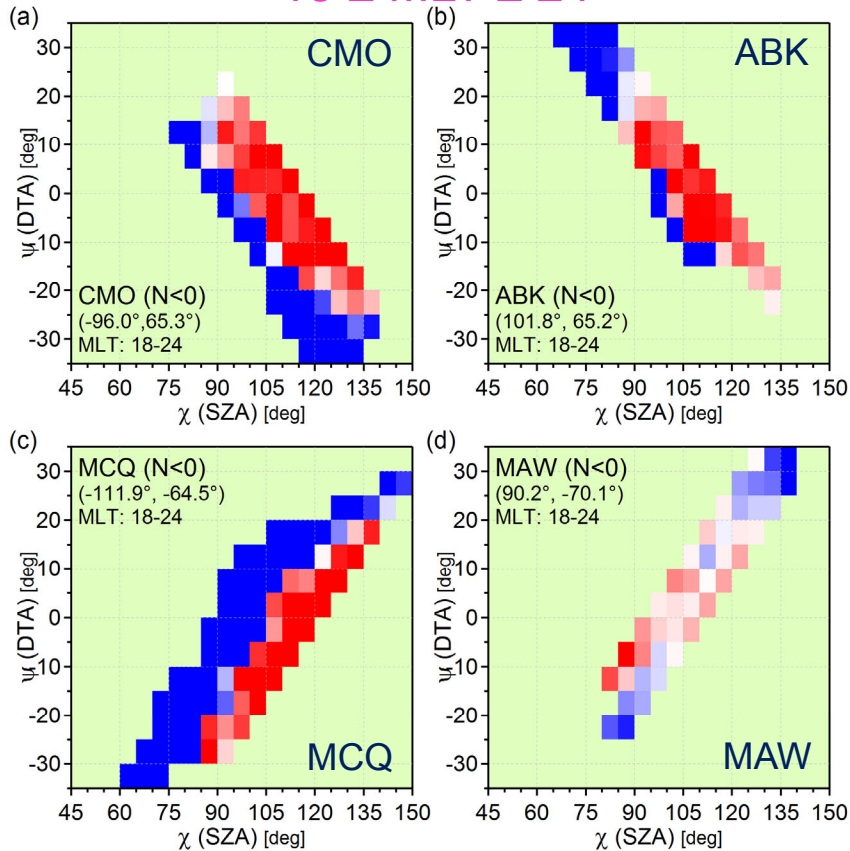


DTA & SZA are correlated but with **different offsets**

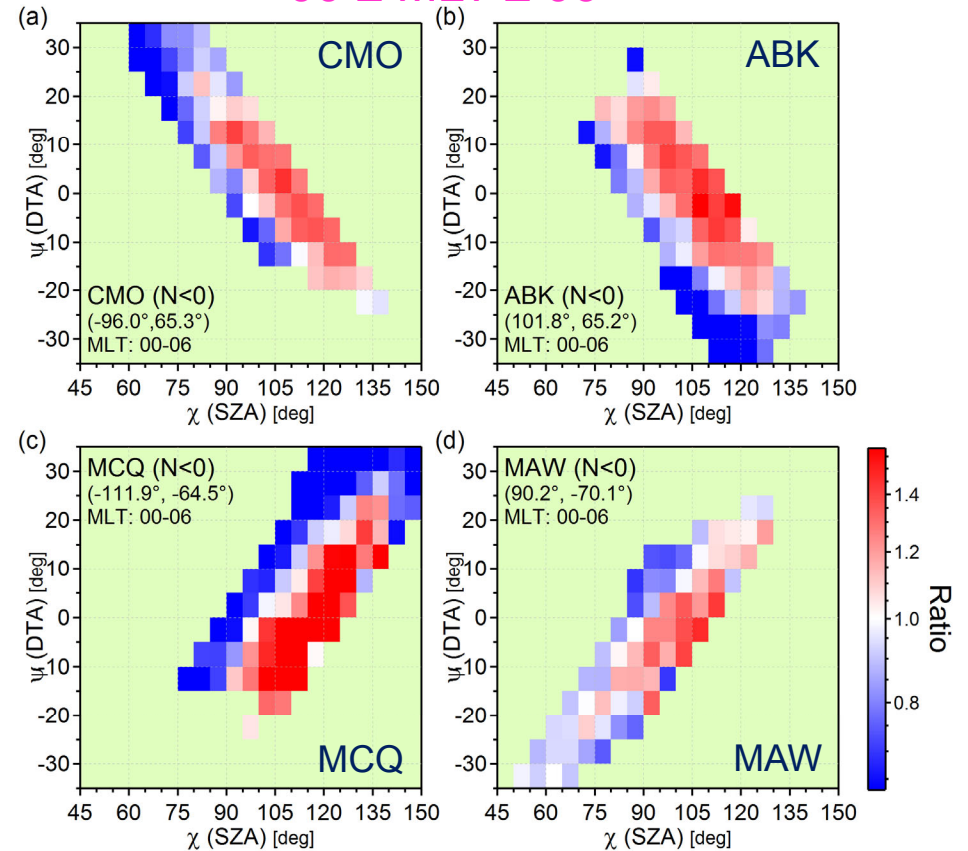


WEJ is more intense for larger SZA and larger |DTA|

18 ≤ MLT ≤ 24

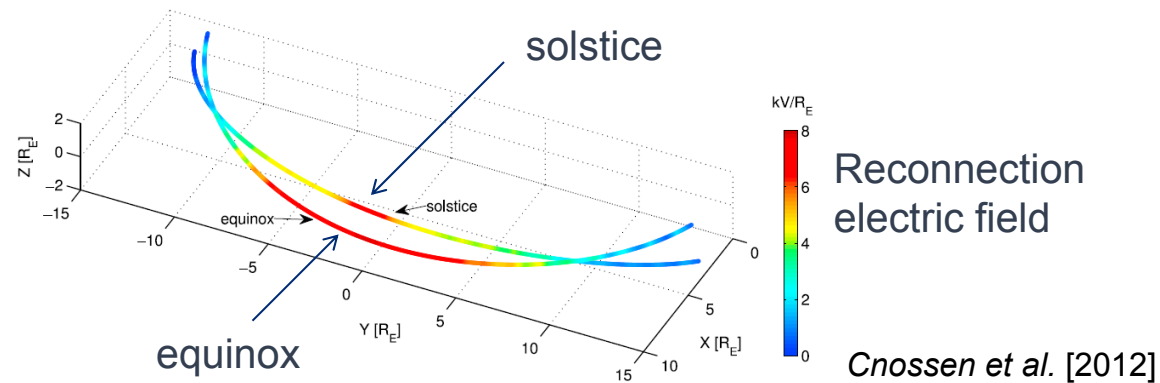


00 ≤ MLT ≤ 06



Why is the WEJ weaker when the DTA is larger?

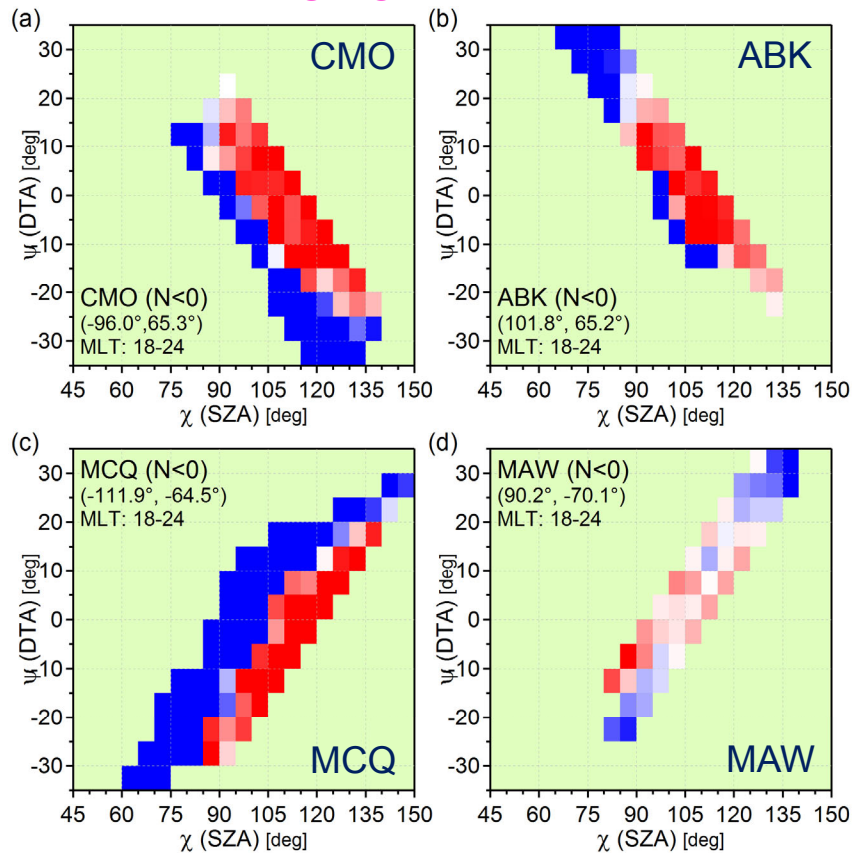
1) The shape of the dayside MP affects the reconnection rate.



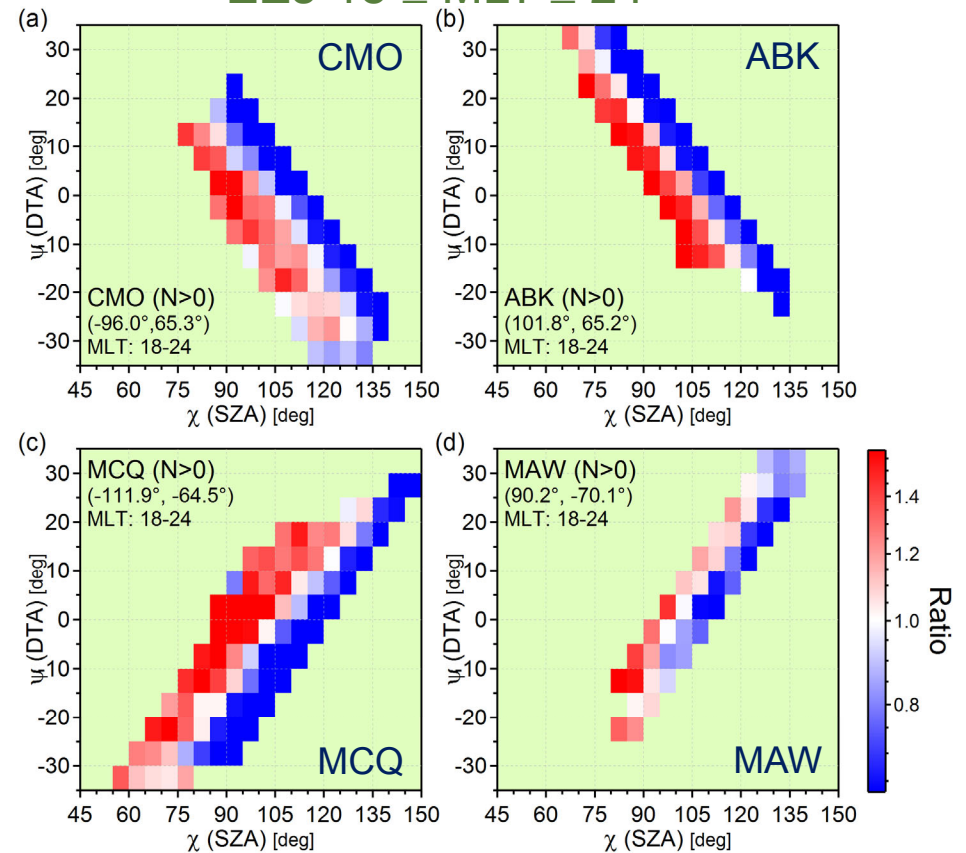
2) The magnetic field at the flanks has a component parallel to the SW, reducing the growth of the KHI.

WEJ/EEJ is more intense in the dark/sunlit hemisphere

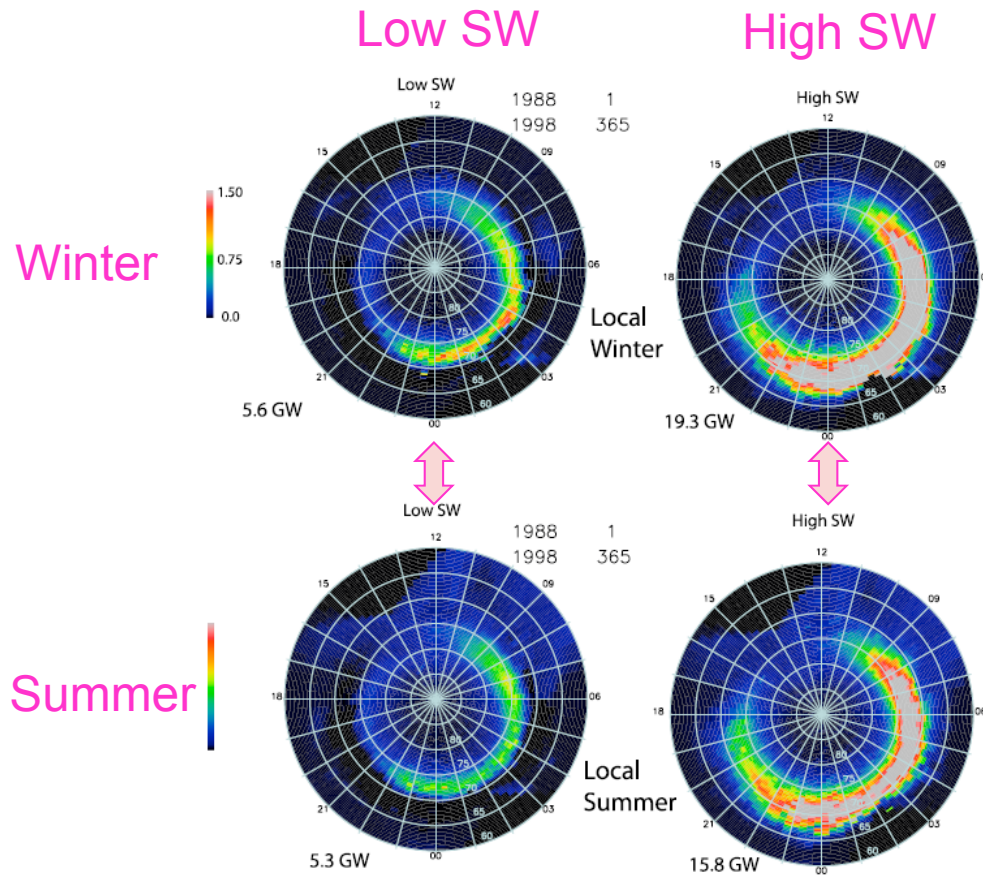
WEJ $18 \leq \text{MLT} \leq 24$



EEJ $18 \leq \text{MLT} \leq 24$



Why is the WEJ stronger when the SZA is larger?



- More intense diffuse precipitation in the dark hemisphere [Hamrin et al., 2005].
- Why?
 - 1) Small field-aligned acceleration?
 - 2) Interhemispheric asymmetry of wave generation/propagation?
 - 3) Secondary electrons from the other hemisphere?

Summary

- The nightside **westward/eastward** electrojet (**WEJ/EEJ**) is more intense when the ionosphere is **dark/sunlit**.
- The auroral electrojet, especially **WEJ**, is more intense when the dipole tilt is smaller, and this effect is comparable to the effect of solar illumination.
- The preference of the **WEJ** intensity for the dark ionosphere likely reflects that of diffuse e- precipitation and ionospheric conductance.



JOHNS HOPKINS
APPLIED PHYSICS LABORATORY

JGR Space Physics

RESEARCH ARTICLE

10.1029/2019JA026707

Key Points:

- The nightside westward electrojet (WEJ) is more intense when the ionosphere is dark, and the eastward electrojet (EEJ) when it is sunlit
- Both WEJ and EEJ are more intense when the dipole tilt is smaller, and this effect is comparable to the effect of solar illumination
- The preference of the WEJ intensity for the dark ionosphere likely reflects that of diffuse e- precipitation and ionospheric conductance

Correspondence to:

S. Ohtani,
ohtani@jhuapl.edu

Citation:






Ohtani, S., Gjerloev, J. W., Johnsen, M. G., Yamauchi, M., Brändström, U., & Lewis, A. M. (2019). Solar illumination dependence of the auroral electrojet intensity: Interplay between the solar zenith angle and dipole tilt. *Journal of Geophysical Research: Space Physics*, 124. <https://doi.org/10.1029/2019JA026707>

Received 7 MAR 2019

Accepted 11 JUL 2019

Accepted article online 18 JUL 2019

Solar Illumination Dependence of the Auroral Electrojet Intensity: Interplay Between the Solar Zenith Angle and Dipole Tilt

S. Ohtani¹ , J. W. Gjerloev^{1,2} , M. G. Johnsen³ , M. Yamauchi⁴ , U. Brändström⁴ , and A. M. Lewis⁵

¹The Johns Hopkins University Applied Physics Laboratory, Laurel, MD, USA, ²Faculty for physics and technology, University of Bergen, Bergen, Norway, ³Tromsø Geophysical Observatory, UiT the Arctic University of Norway, Tromsø, Norway, ⁴Swedish Institute of Space Physics, Kiruna, Sweden, ⁵Geoscience Australia, Canberra, ACT, Australia

Abstract The present study investigates the dependence of the local auroral electrojet (AEJ) intensity on solar illumination by statistically examining northward geomagnetic disturbances in the auroral zone in terms of the solar zenith angle χ . It is found that on the dayside, both westward and eastward electrojets (WEJ and EEJ) are more intense for smaller χ , suggesting that the solar extreme ultraviolet-induced conductance is the dominant factor for the AEJ intensity. On the nightside, in contrast, the χ dependence of the AEJ intensity, if sorted solely by the magnetic local time, apparently depends on the station longitude and hemisphere. However, if additionally sorted by the dipole tilt angle ψ , a consistent pattern emerges. That is, although χ and ψ are correlated, the solar zenith angle and dipole tilt angle have physically different effects on the AEJ intensity. The nightside AEJ, especially the WEJ, tends to be more intense for smaller $|\psi|$. Moreover, whereas the WEJ is statistically more intense when the ionosphere is dark, the EEJ is more intense when it is sunlit. The preference of the WEJ for the dark ionosphere prevails widely in magnetic local time from premidnight to dawn, and therefore, it cannot be attributed to the previously proposed processes of the preferred monoenergetic or broadband auroral precipitation in the dark ionosphere. Instead, it may be explained, at least morphologically, in terms of the conductance enhancement due to the diffuse auroral precipitation, which is also prevalent from premidnight to dawn and is more intense in the dark hemisphere.

1. Introduction

Solar illumination affects the electrodynamic coupling between the magnetosphere and ionosphere in various ways. On the dayside the large-scale field-aligned currents (FACs), Region 1 (R1) and Region 2 (R2) currents, are noticeably stronger (i.e., the FAC density is larger) and more intense (i.e., the FAC intensity is larger) in the summer/sunlit hemisphere than in winter/dark hemisphere (e.g., Coxon et al., 2016; Fujii et al., 1981; Haraguchi et al., 2004; Ohtani, Ueno, & Higuchi, 2005; Ohtani, Ueno, Higuchi, & Kawano, 2005; Wang et al., 2005), which can be attributed to the higher ionospheric conductance of the summer/sunlit hemisphere due to solar extreme ultraviolet (EUV) radiation.

On the nightside, in contrast, the R1 and R2 currents are statistically more intense in the winter/dark hemisphere (Ohtani, Ueno, & Higuchi, 2005; Ohtani, Ueno, Higuchi, & Kawano, 2005; Ohtani et al., 2009) and so is auroral precipitation (Newell et al., 1996, 2010) and emission (Liou et al., 2001). It appears that once the FAC intensifies, the ionospheric conductance in the dark hemisphere becomes higher than that in the sunlit hemisphere due to more intense and energetic electron precipitation, overcompensating the absence of solar EUV radiation in the dark hemisphere (Ohtani et al., 2009).

In the present study we seek to advance our understanding of the solar illumination effect on the magnetosphere-ionosphere (M-I) system by examining the local intensity of the auroral electrojets (AEJs). An emphasis is placed on the nightside. One might expect, based on the aforementioned inter-hemispheric asymmetries of the FAC intensity and auroral acceleration, that the nightside AEJs would be more intense in the dark hemisphere. However, we find in this study that the M-I system behaves in a more complex way, and this expectation is only partially correct.

We use the solar zenith angle (SZA) χ as a measure of the local solar illumination. The local solar EUV energy input changes more significantly as a function of the SZA than the solar EUV irradiance (i.e., solar

Table 1
Ground Magnetometer Stations and Their Coordinates and Data Periods

Station	Code	MLon	MLat	Geo Lon	Geo Lat	Period
Bear Island	BJN	108.2	71.5	19.2	74.5	1987–2017
Soerøya	SOR	106.2	67.3	22.2	70.5	1996–2017
Tromsø	TRO	103.0	66.6	18.9	69.7	1988–2017
Abisko	ABK	101.8	65.2	18.8	68.4	1979–2017
Kiruna	KIR	102.7	64.6	20.4	67.8	1995–2017
Sodankylä	SOD	107.3	63.8	26.6	67.4	1980–2017
College	CMO	−96.0	65.3	212.1	64.9	1976–2017
Macquarie Island	MCQ	−111.9	−64.5	159.0	−54.5	1992–2017
Mawson	MAW	90.2	−70.1	62.9	−67.6	1991–2017

Note. MLons and MLats are in the Altitude-Adjusted Corrected Geomagnetic (AACGM) coordinates based on the International Geomagnetic Reference Field (IGRF) 2000 model.

phase) itself. Nevertheless, it is highly unlikely, especially for the nightside AEJs, that the solar illumination is the dominant controlling factor of the AEJ intensity. It would be ideal if we can examine the AEJ intensity with other internal and external conditions fixed, which, however, is not feasible. Therefore, for examining its dependence on the solar illumination, or on χ as we do in this study, we need to carefully take into account external and internal factors that may affect the AEJ intensity. Here we make four points regarding such factors.

First, the AEJ intensity may depend on the solar illumination in different ways for different intensities of the external driving. If the external driving is so weak that the contribution of auroral precipitation to the ionospheric conductance is negligible, the ionospheric conductance would be higher in the sunlit hemisphere than in the dark hemisphere, and accordingly, the AEJs would be more intense in the sunlit hemisphere. On the other hand, if the AEJ is more intense in the dark ionosphere, the absence of the solar EUV contribution needs to be overcompensated by more intense auroral precipitation, which requires a certain level of external driving.

Second, it is possible that the eastward electrojet current (EEJ) and westward electrojet current (WEJ) depend on the solar illumination differently because they are distributed in different magnetic local time (MLT) sectors, and accordingly, the characteristics of the associated precipitation are different. The EEJ extends from afternoon to midnight, where monoenergetic electron precipitation prevails (e.g., Lin & Hoffman, 1979), but other types of auroral precipitation coexist especially in the premidnight sector (e.g., Newell et al., 2009). The substorm-associated WEJ at premidnight is also characterized by the coexistence of various types of auroral precipitation. In contrast, the WEJ associated with the global two-cell convection is centered at dawn, where diffuse precipitation is dominant.

Third, the latitude of the auroral oval is a function of MLT, and it also depends on the state of the M-I system such as the substorm phase. It is possible that if we examine the AEJ intensity measured at a single station, and therefore, at a fixed magnetic latitude (MLat), the measurements are biased to a particular state of the M-I system, and this bias itself may be different at different MLTs. In addition, the SZA changes as a function of MLT. Therefore, various factors are linked with each other. One promising approach to resolving this complexity, which we adopt in this study, is to use data from stations at different MLats and magnetic longitudes (MLons) and to deduce consistent features.

Finally, related to the previous point, we need to pay special attention to the dipole tilt angle (DTA) ψ , which is the complement of the angle between the terrestrial dipole axis and the Sun-Earth line ($\psi > 0$ in northern summer and < 0 in northern winter). It has been widely known that geomagnetic activity as measured by various indices tends to be higher when $|\psi|$ is smaller (e.g., Cliver et al., 2000; Svalgaard, 1977). Since the SZA(χ) and DTA(ψ) are generally correlated with each other, it is possible that the local AEJ intensity depends on χ through ψ .

The rest of this paper is organized as follows. In section 2 we briefly describe the ground magnetometer data that we use in this study. In section 3 we statistically examine the geomagnetic disturbance in terms of MLT, SZA(χ), and DTA(ψ). The result is discussed in section 4. In section 5 we summarize the overall study.

2. Data Set

In the present study we use ground magnetometer data from various stations, which are listed in Table 1 along with their coordinates and the periods of data. First we examine data from Abisko (ABK). ABK is a part of the International Monitor for Auroral Geomagnetic Effects (IMAGE) network, and it is one of the 12 stations that are used for deriving the auroral electrojet (AE) index. We then extend our analysis to other IMAGE stations at different MLats, which range from 63.8° to 71.5°. Finally, we examine data from three more stations located in different areas of the world. College (CMO) is another AE station, which is located

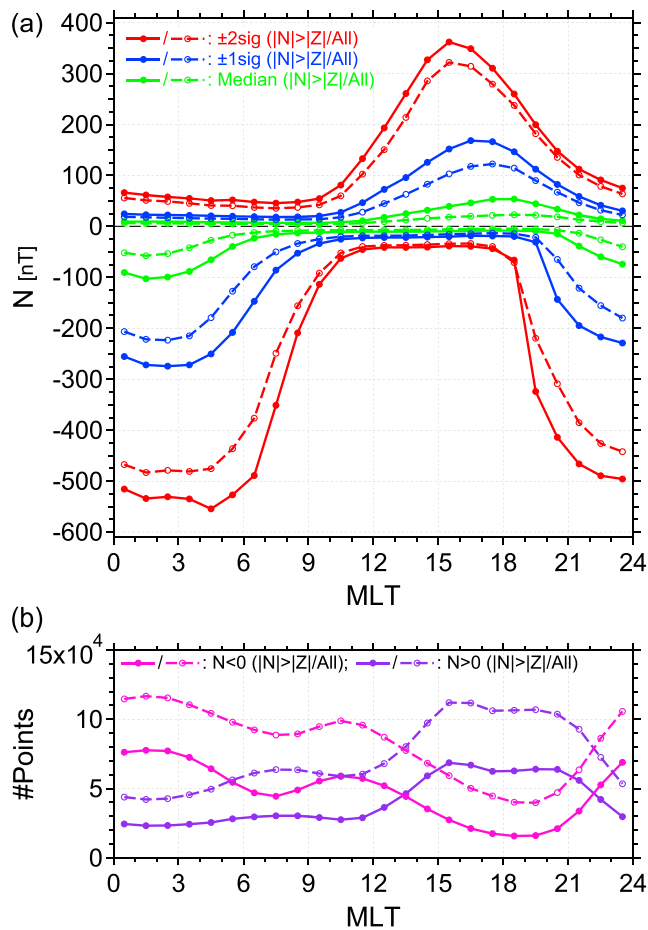


Figure 1. (a) Median (green), -1σ (blue), and -2σ (red) of negative N and median (green), $+1\sigma$ (blue), and $+2\sigma$ (red) of positive N observed at ABK and (b) the number of 5-min averages for negative (magenta) and positive (purple) N as a function of MLT. The dashed lines are for the entire data set, and the solid lines are for the subset with $|N| > |Z|$ for each sign of N .

the entire data set, whereas the solid lines are for the subset of data points with $|N| > |Z|$. Figure 1b shows the numbers of 5-min data points for this subset (solid) and the entire data set (dashed) for negative (magenta) and positive (purple) N . We have a total of ~ 3.76 million 5-min data points, among which $|N| > |Z|$ for ~ 2.12 million points, $N < 0$ for ~ 1.14 million points, and $N \geq 0$ for ~ 0.98 million points.

N tends to be negative on the dawnside corresponding to the WEJ, and it tends to be positive in the dusk sector corresponding to the EEJ. The overall distribution is consistent with the global two-cell pattern of equivalent currents, which is known as the DP2 system (Nishida, 1968). The demarcation between negative and positive N disturbances is sharp on the dayside (the lines are confined in a narrow vertical range), and it takes place at prenoon, at MLT = 10–12, as expected from the dawnward shift of the throat area (e.g., Heppner & Maynard, 1987). On the nightside, in contrast, negative and positive N disturbances coexist in the evening-to-midnight sector, which presumably reflect the substorm-related enhancement of the WEJ (e.g., Akasofu et al., 1965). N tends to be larger in magnitude with the condition $|N| > |Z|$ as this condition favors AEJs flowing near the latitude of the ground station. In the rest of this paper we will primarily use this subset for ABK, as well as for other stations.

Figures 2a and 2b show the number of ABK 5-min data points for negative and positive N , respectively, in the MLT-SZA(χ) frame. The overall distribution is V-shaped (rotated clockwise by 90°). In the midday sector, χ can be as small as $\sim 45^\circ$, whereas in the midnight sector, it can be as large as $\sim 135^\circ$. At a given MLT, χ varies by 50 – 55° because of the precession of Earth's rotation axis. Corresponding to the

in Alaska on the other side of Earth from ABK. Macquarie Island (MCQ) and Mawson (MAW) are in the same MLon sectors as CMO and ABK, respectively, but in Southern Hemisphere.

We use 5-min averages of geomagnetic disturbances observed at each station, which we created from 1-min data provided through SuperMAG; for the SuperMAG database, the baseline, which includes diurnal variations, annual variations, and offsets, is subtracted, and data are given in the NEZ local magnetic coordinate system (Gjerloev, 2012). For any practical purpose the N and E components can be regarded as perturbations in the H (northward) and D (eastward) directions, respectively, and Z is directed vertically down.

In the present study we use the N component magnetic disturbance, N , as a measure of the local AEJ intensity; N is positive for the EEJ and negative for the WEJ. In general, the orientation of the AEJ is not perpendicular to the N direction for various reasons such as the antisunward shift of the auroral oval relative to the magnetic pole and geomagnetic activity (e.g., substorms). The locality of the geomagnetic field also affects the orientation of N (e.g., Laundal & Gjerloev, 2014). However, our analysis concerns the SZA dependence of N at individual stations, and therefore, the result is not sensitive to the selection of the coordinate system. We also note that the EEJ and WEJ as we examine in this study are equivalent currents. However, in the auroral zone, the overhead ionospheric current, more precisely, its divergence-free part, is usually the primary contributor to the equivalent currents. In addition, we require $|N| > |Z|$ in this study so that the AEJs tend to be located around the latitudes of the ground stations.

3. Data Analysis

We first examine the MLT distribution of N at ABK. For each 1-hr wide MLT bin we calculated the median and the central 68.3 and 95.4 percentiles for negative and positive N separately, which we simply denote as $\pm 1\sigma$ and $\pm 2\sigma$; σ would correspond to the standard deviation if the distribution is normal. Figure 1a shows the median, -1σ and -2σ for negative N and the median and $+1\sigma$ and $+2\sigma$ for positive N . The dashed lines are for

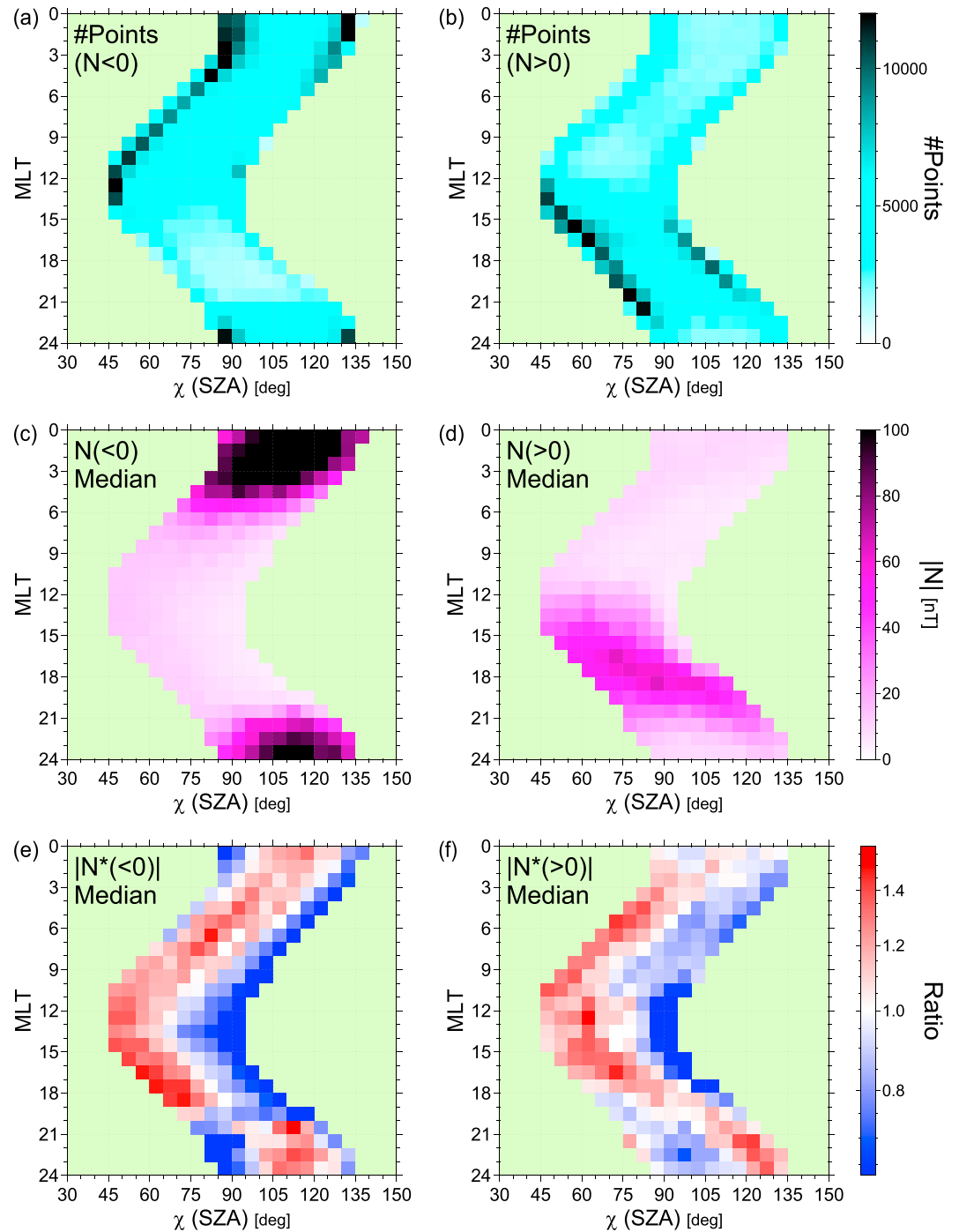


Figure 2. The MLT-SZA(χ) diagrams of (a, b) the number of 5-min averages, (c, d) the medians of N , and (e, f) $|N^*|$ for ABK. N^* is the N value of each cell normalized by its average over the corresponding 1-hr-wide MLT bin. The left and right columns are for negative and positive N , respectively.

distribution of N (Figure 1), the negative and positive data points are distributed most densely in the premidnight-to-prenoon and postnoon-to-premidnight sectors, respectively. In those favorable MLT sectors the number of data points in each $1 \text{ hr} \times 5^\circ$ cell ranges from $\sim 3,000$ in the middle of the V-shaped band to $\sim 15,000$ near its edges. At other MLTs it is typically 1,500–5,000. The number of data points tend to be larger closer to the edges of the χ range since the tilt angle of Earth's rotation axis changes most slowly around the solstices; the one or two leftmost and rightmost cells include a few

months' worth of data around the solstices of each year, and the rest of the data are distributed widely between them (not shown).

Figures 2c and 2d show the medians of negative and positive N in the same format. The magnitude of negative N tends to be large in the late premidnight-to-dawn sectors, whereas the magnitude of positive N tends to be large in the postnoon-to-late evening sector, which is consistent with the result of Figure 1.

Both negative and positive N distributions appear to have structures in the MLT-SZA(χ) frame. To make the χ dependence stand out, we normalized, for each 1-hr-wide MLT bin, the value of each cell by the average magnitude of that MLT bin. Hereafter, we denote this normalized N as N^* , and we examine its magnitude $|N^*|$. The results are shown in Figures 2e and 2f for negative and positive N^* , respectively. In each figure the color is reddish and bluish for $|N^*| > 1$ and < 1 , respectively, and the gradation represents its extent.

On the dayside (MLT = 06–18), for both negative and positive N^* , the left half of the V-shaped band is reddish, whereas the right half is bluish indicating that the AEJs are more intense when the SZA is smaller. The tendency is the opposite in the dusk-to-midnight sector, where both negative and positive N^* tend to be larger in magnitude for larger χ . For negative N^* , the transition between the red-to-blue and blue-to-red patterns takes place sharply at MLT = 20. For positive N^* , in contrast, the transition is gradual. In the midnight-to-dawn sector (MLT = 00–06), negative N^* apparently prefers the intermediate range of χ , whereas positive N^* shows the red-to-blue pattern. We note that N^* reveals systematic patterns even for the MLT sectors where the occurrence is far less frequent than in the other sectors, that is, MLT = 06–21 for negative N (Figure 2c) and MLT = 00–12 for positive N (Figure 2d).

We examined -1σ and -2σ of negative N and $+1\sigma$ and $+2\sigma$ of positive N in the same way. The results, as shown in Figure 3, are more structured than those for the medians, and there are some noticeable differences. First, for negative N , the demarcation between the red-to-blue and blue-to-red patterns shifts to earlier MLTs from MLT = 20 for the median to MLT = 19 for -1σ (Figure 3a) and to MLT = 18 for -2σ (Figure 3c). Note also that in Figure 1a the range of negative N in the premidnight sector extends duskward as its magnitude increases. We therefore suggest that the preference of negative N for large χ in the premidnight sector is related to the enhancement of geomagnetic activity (e.g., substorms). Second, for positive N in the midnight-to-dawn sector (MLT = 00–06), the red-to-blue pattern, which we found for the median, has almost disappeared for $+1\sigma$, and the pattern is apparently reversed for $+2\sigma$ showing the blue-to-red pattern. In that MLT sector N is positive far less frequently than it is negative (Figures 1 and 2d). However, when N becomes positive and large there, its χ dependence is similar to that of negative N in the premidnight sector, which also suggests that the blue-to-red pattern is a feature of active periods.

As a measure of the external driver, we use the Z component of the interplanetary magnetic field (IMF), IMF B_Z , which we averaged over 60 to 5 min before the start of each 5-min ground magnetometer data point. Here we used OMNI data set, for which the IMF measurements are already time shifted to the nose point of the bow shock. We grouped the ABK data into three groups, southward (IMF $B_Z \leq -1$ nT), small in magnitude ($-1 < \text{IMF } B_Z < +1$ nT), and northward ($+1 \text{ nT} \leq \text{IMF } B_Z$); each subset includes a roughly equal number (0.47–0.53 million) of data points. We calculated N^* for each subset, and the result is shown in Figure 4. Whether N^* is negative (left) or positive (right), the patterns for the northward (top) and small-magnitude (middle) IMF B_Z are similar to each other, and they are also similar to those for the median (Figures 2e and 2f). In contrast, the patterns for the southward IMF B_Z (bottom) resemble those for -1σ of negative N (Figure 3a) and $+1\sigma$ of positive N (Figure 3b). This result is reasonable since, in general, geomagnetic activity is well correlated with the preceding IMF B_Z condition.

We conducted the same analysis for five more ground magnetometer stations in the Scandinavian sector, the MLats of which range from 63.8° (SOD) to 71.5° (BJN); see Table 1. Figures 5 and 6 show the result for negative and positive N^* , respectively, in the descending order of the MLat from the top. Here we included the result for ABK (fourth row) for comparison. The left, middle, and right columns are for the southward (IMF $B_Z \leq -1$ nT), small-magnitude ($-1 < \text{IMF } B_Z < +1$ nT), and northward ($+1 \text{ nT} \leq \text{IMF } B_Z$) IMF B_Z conditions, respectively.

As we found for ABK, for each station and for each sign of N^* , the patterns are similar for the small-magnitude (middle) and northward (right) IMF B_Z . At least they are far less different from each other than from the pattern for the southward IMF B_Z (left). Also for each IMF B_Z condition and for each sign of N^* , the

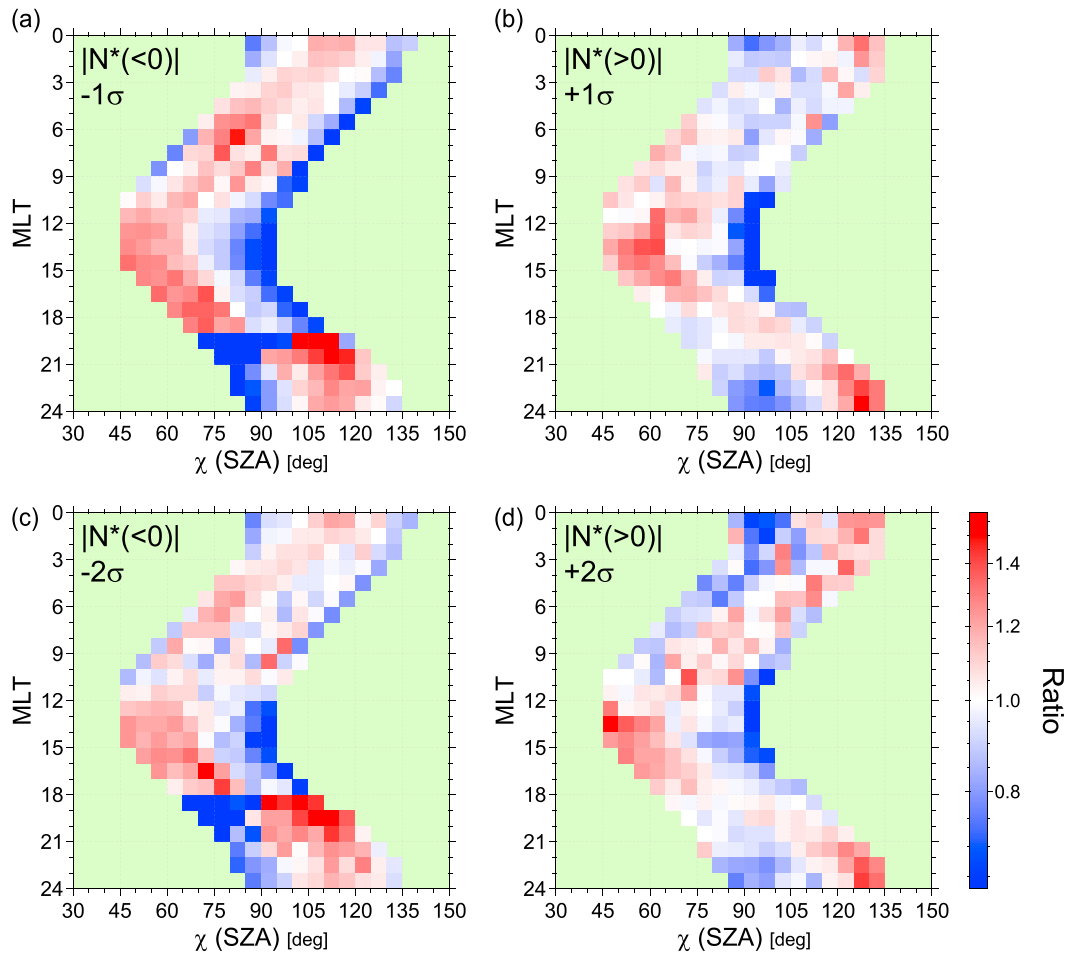


Figure 3. The MLT-SZA(χ) diagrams of $|N^*|$ for (a) -1σ of negative N , (b) $+1\sigma$ of positive N , (c) -2σ of negative N , and (d) $+2\sigma$ of positive N .

overall patterns are basically consistent among the stations but with some differences for BJN, the most poleward station. For the midday sector, for example, the preference for smaller χ (i.e., the red-blue pattern) can be found in each panel, although the red versus blue contrast and the corresponding MLT range are not exactly the same.

Of our interest is the preference for larger χ (i.e., the blue-to-red pattern) in the premidnight sector. In general, it is more noticeable for negative N^* than for positive N^* as we found for ABK. For negative N^* , the MLT sector of the preference extends more duskward for southward IMF B_z than for the other two IMF B_z conditions. The exception is BJN (top row of Figure 5), for which this preference is most evident for the northward IMF B_z . This might correspond to substorms that take place when the auroral oval is contracted (Lui et al., 1976). It may also reflect the AEJ during the substorm recovery phase, during which the poleward edge of the nightside auroral oval can reach the MLat of BJN.

Now we extend our analysis to three more stations, which are located in different areas, that is, CMO, MCQ, and MAW; see Table 1. CMO is also located in the northern auroral zone but on the opposite side of Earth from ABK. MCQ is in the same sector as CMO, 15.9° east of CMO, but in Southern Hemisphere. MAW is in the same sector as ABK, 11.6° east of ABK, and is also in Southern Hemisphere, but higher in MLat, -70.1° . In this part of the study we focus on the southward (IMF $B_z \leq -1$ nT) IMF condition.

Figure 7 shows the MLT-SZA(χ) diagrams of those three stations and ABK for negative N^* . The four panels are arranged in such a way that they reflect the relative locations of the four stations. One may expect that the diagram of each station is similar to that of ABK. However, Figure 7 shows noticeable differences among the stations. For $N^* < 0$, the red-to-blue pattern we found for the dawnside of ABK can also be

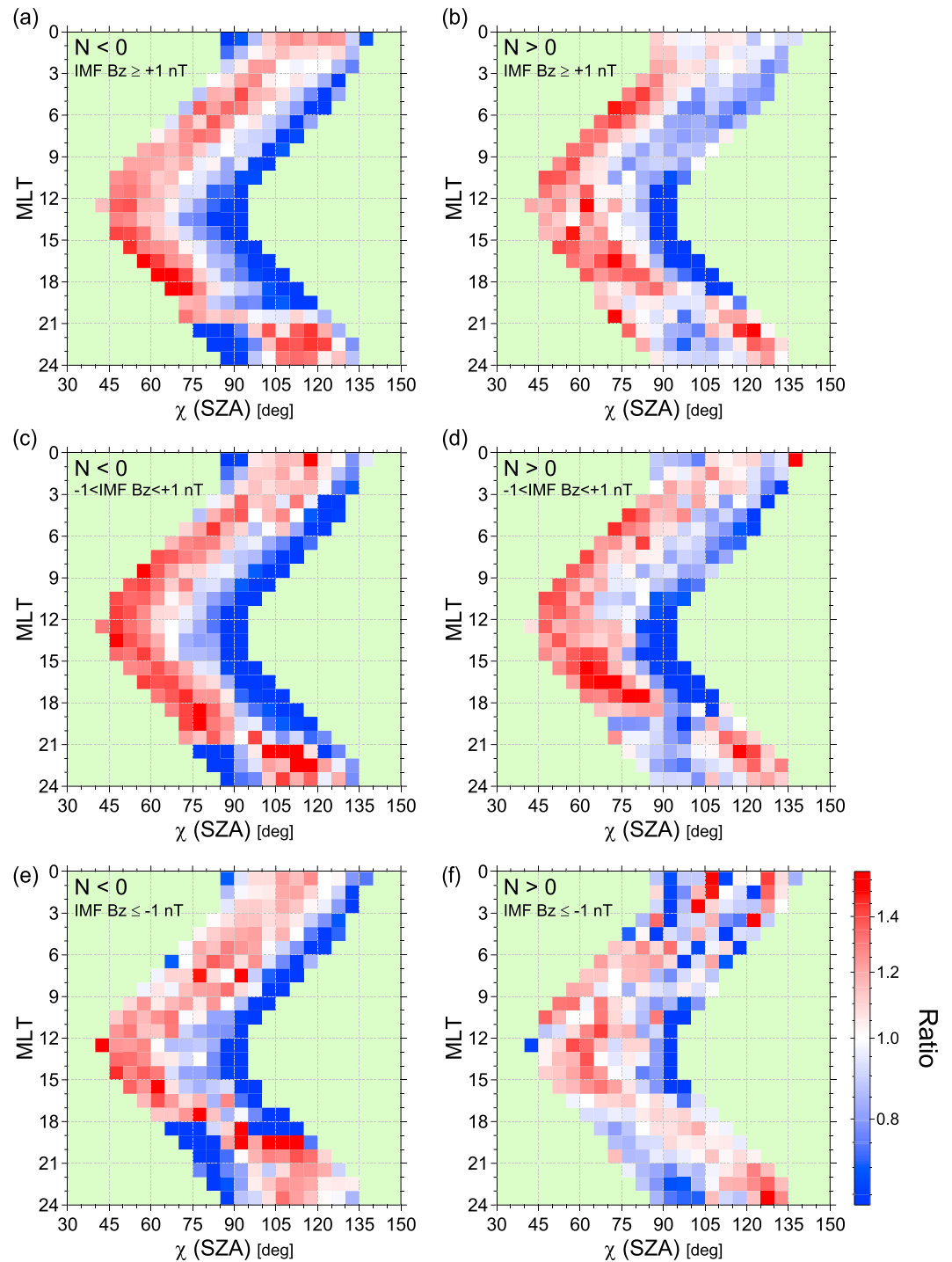


Figure 4. The MLT-SZA(χ) diagrams of (left) negative and (right) positive N^* for (top) northward ($+1 \text{ nT} \leq \text{IMF } B_z$), (middle) small magnitude ($-1 < \text{IMF } B_z < +1 \text{ nT}$), and (bottom) southward ($\text{IMF } B_z \leq -1 \text{ nT}$) IMF B_z .

found for MCQ. However, for CMO the pattern is just the opposite, and for MAW, N^* is apparently larger in the intermediate range of χ . Moreover, the blue-to-red pattern in the premidnight sector, which we found for ABK, cannot be found for any of the other three stations. In fact, for those three stations the pattern is more like red-to-blue than blue-to-red in the premidnight sector.

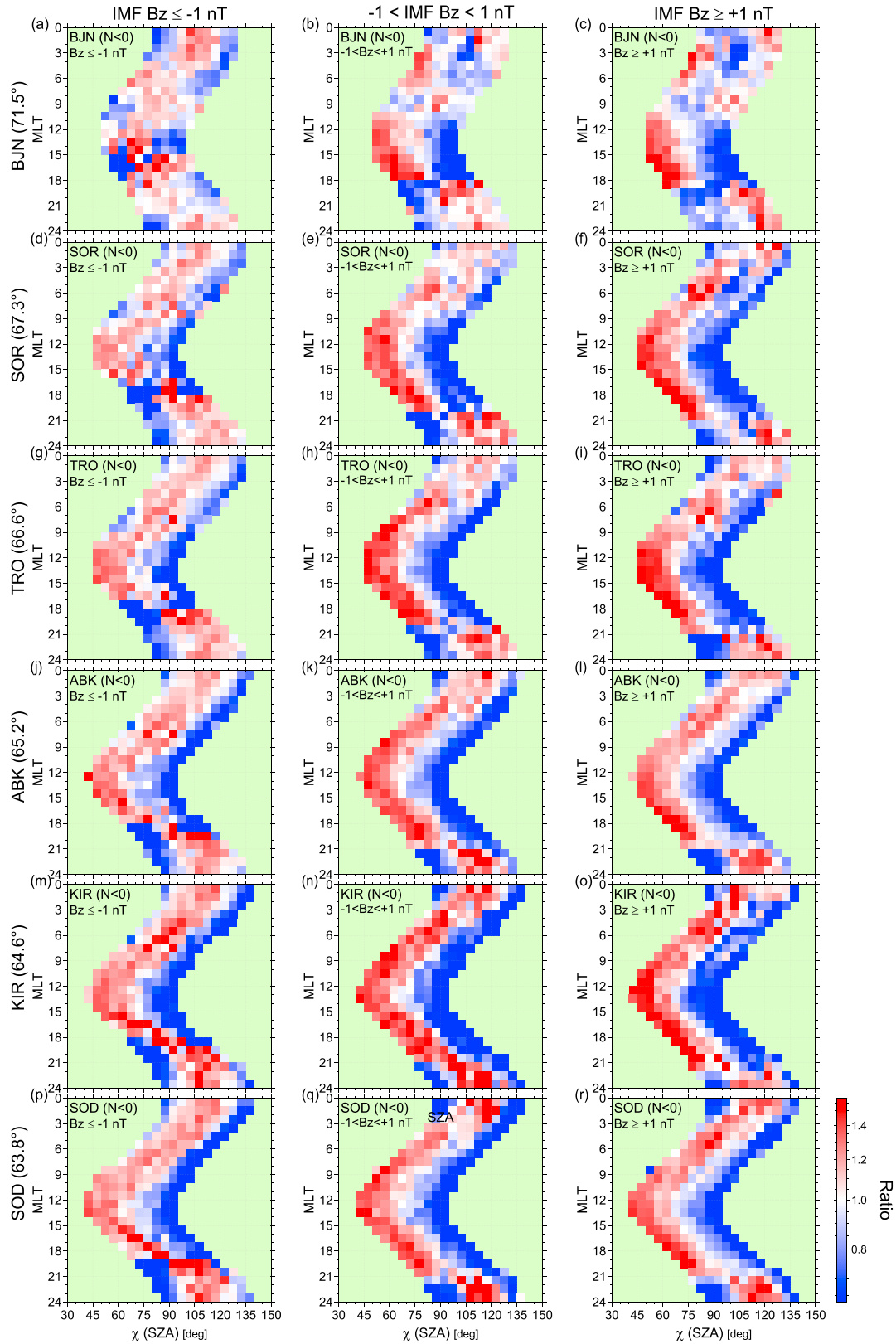


Figure 5. The MLT-SZA(χ) diagrams of negative N^* at (first row) BJN, (second) SOR, (third) TRO, (fourth) ABK, (fifth) KIR, and (sixth) SOD for (left) southward (IMF $B_z \leq -1$ nT), (middle) small magnitude ($-1 < \text{IMF } B_z < +1$ nT), and (right) northward ($+1 \text{ nT} \leq \text{IMF } B_z$) IMF B_z .

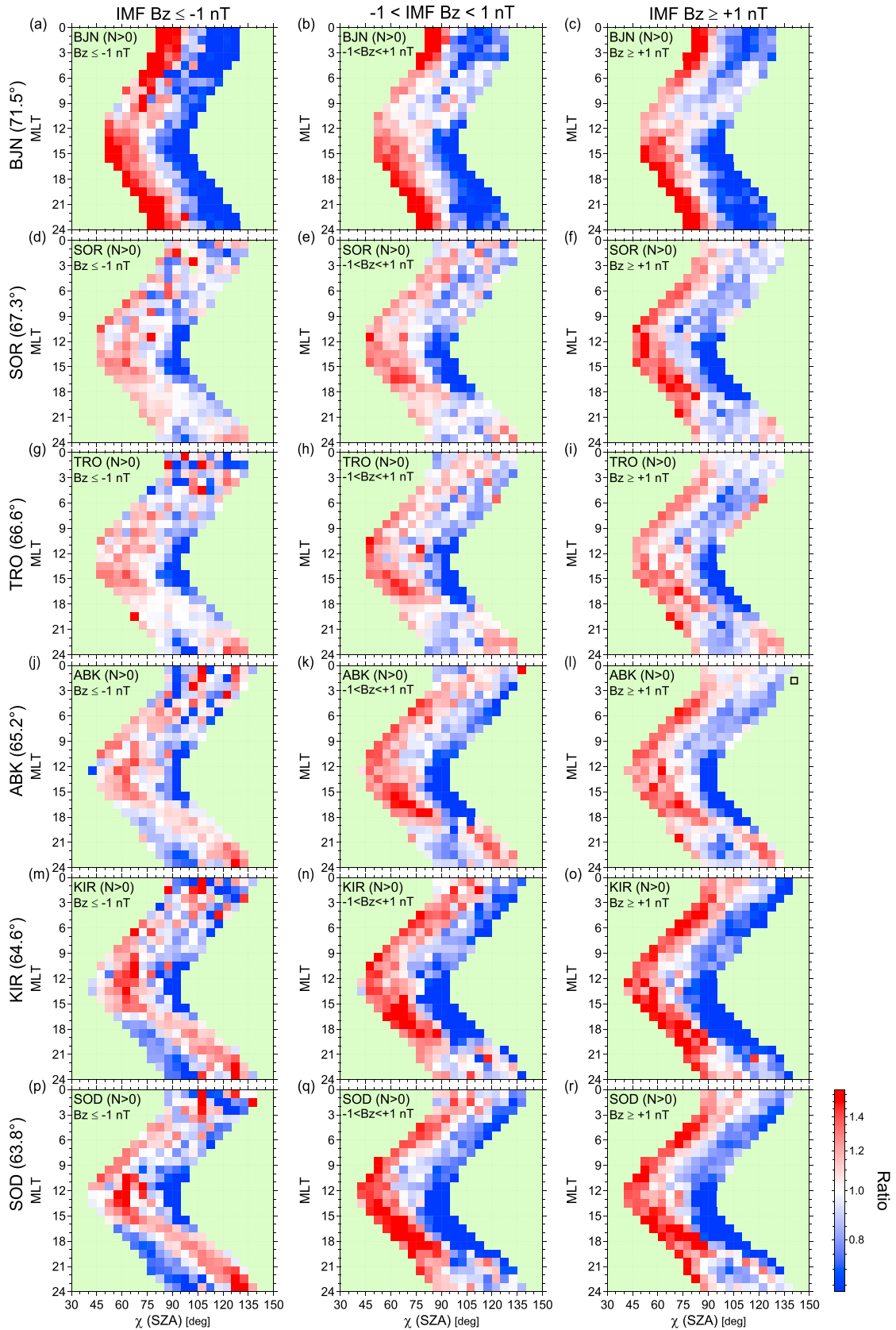


Figure 6. Same as Figure 5 but for positive N^* .

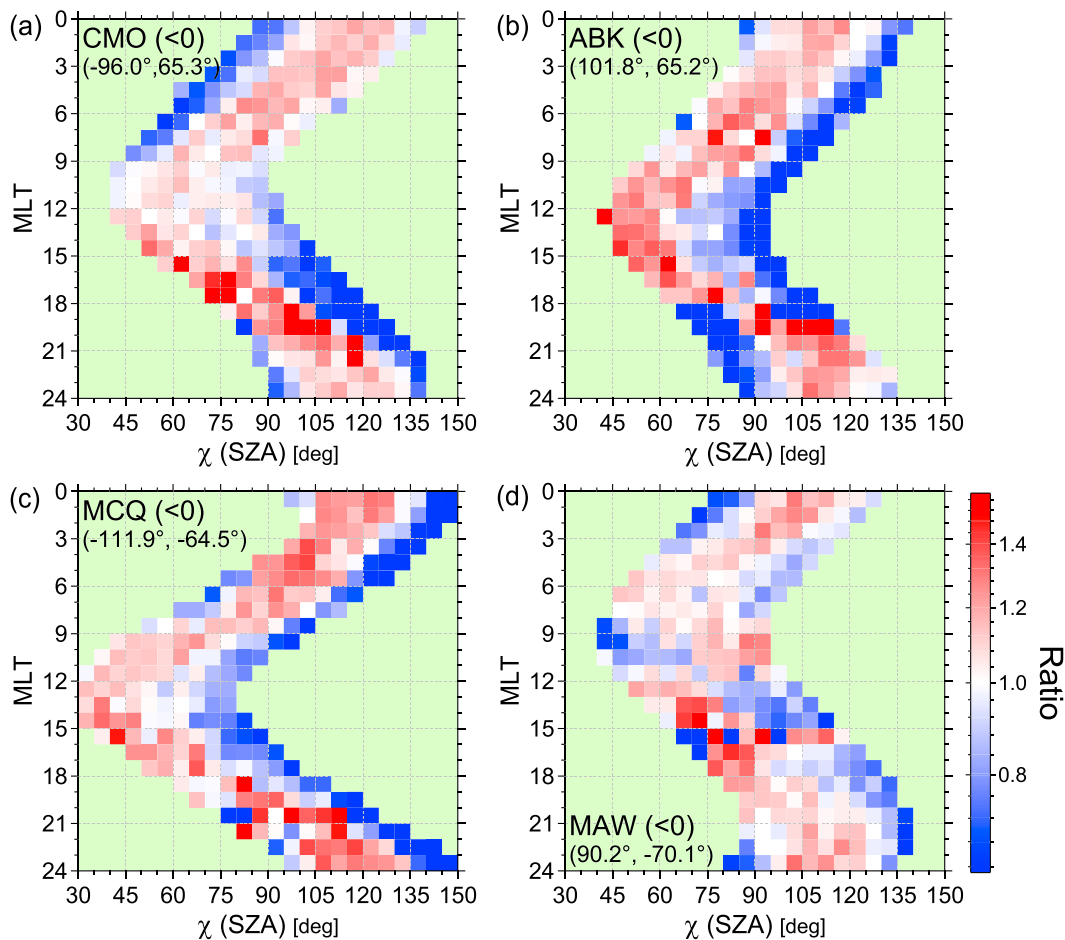


Figure 7. The MLT-SZA(χ) diagrams of negative N^* at (a) CMO, (b) ABK, (c) MCQ, and (d) MAW for the southward IMF (IMF $B_z \leq -1$ nT) condition.

Figure 8 shows the result for positive N^* in the same way as Figure 7. For positive N^* , we can find more overall similarities than differences among ABK, CMO, and MCQ especially for the postnoon-to-midnight sector, where positive N is prevalent. The result for MAW is noticeably distinct, which clearly shows the red-to-blue pattern with an apparent exception for a few MLT bins at prenoon, and it is akin to that for BJN for $N^* > 0$ (Figure 6a). Note that both MAW and BJN are located poleward of the nominal latitude of the nightside auroral oval. Thus, for positive N^* , the MLT-SZA(χ) diagram is apparently consistent with the result for the Scandinavian chain (Figure 6).

It is improbable that the variability among those stations for negative N^* arises from statistical insignificance or a bias to any particular geomagnetic condition. Note that the data of each station cover more than one solar cycle (Table 1), and regarding ABK, its MLT-SZA(χ) pattern is consistent with the patterns of the other auroral zone stations in the same sector (Figures 5 and 6). The result of Figure 7 strongly suggests that there is an additional factor, other than the SZA, that statistically affects the N magnitude so much that it obscures, or even reverse, the SZA(χ) dependence (if the data are binned by MLT as we have done).

The first hypothesis we tested was that for a given MLT the solar illumination of the conjugate point is different depending on the longitude of the station, and it affects the magnitude of N . This hypothesis turned out to be false (not shown). In fact, it is not conceivable that the SZA dependence is reversed depending on the solar illumination of the conjugate point. However, this exercise reminded us that the DTA changes significantly ($\sim 20^\circ$) during a day. In other words, for a given MLT, the corresponding UTs are different for stations at different longitudes and so are the corresponding DTAs. For stations in the same sector, in contrast, the DTA changes with MLT in similar ways. This possibly explains why the MLT- χ diagram is

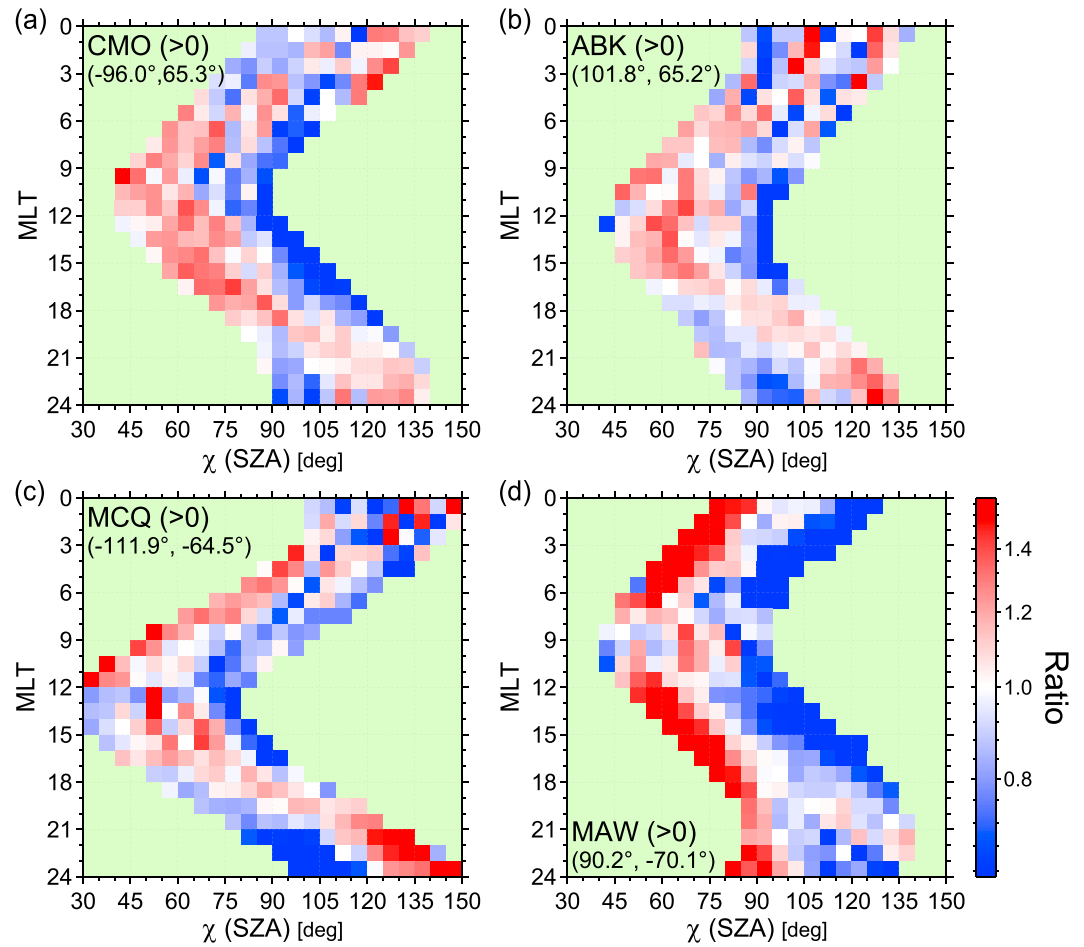


Figure 8. Same as Figure 7 but for positive N^* .

consistent among the auroral-zone stations in the Scandinavian sector (Figures 5 and 6), but it is different for the stations at different longitudes and in different hemispheres (Figures 7 and 8).

In Figures 9–11 we examine the dependence of the N disturbance on the DTA(ψ) and SZA(χ) for the same four stations as we examined in Figures 7 and 8. The median of N of each ψ - χ cell is normalized by its average over all cells in ψ - χ and is shown in color, in reddish and bluish colors above and below the average, respectively. Figure 9 shows the result for negative N in the dusk-to-midnight (MLT = 18 to 24) sector, for which substorms are often responsible. In contrast to Figure 7, we can find overall consistency among the four stations in Figure 9. For CMO and MCQ, although the red-to-blue pattern prevails for the corresponding MLT in Figures 7a and 7c, in Figures 9a and 9c the blue-to-red pattern occupies the middle range of ψ , which is also consistent with the result for ABK (Figure 9b). Most interestingly, N tends to be small for large $|\psi|$ irrespective of its sign. This tendency can be found for each station including MAW (Figure 9d), for which the χ dependence, if at all, is far less clear than for the other three stations. It is therefore suggested that N is partially organized by the DTA(ψ), and the variability of the MLT-SZA(χ) diagrams arises from the fact that different χ bins correspond to different ranges of ψ for different stations; this point will be discussed in more detail in section 4.

Figures 10 and 11 show the results for negative N in the midnight-to-dawn (MLT = 00–06) sector and positive N in the dusk-to-midnight (MLT = 18–24) sector, respectively. Those N disturbances are considered to better reflect the global two cell convection. The consistency among the four stations is again striking in each figure. For negative N (Figure 10) the blue-to-red pattern prevails in the middle range of ψ , and the magnitude of N tends to be smaller for larger $|\psi|$. The result for positive N (Figure 11), in contrast, is characterized

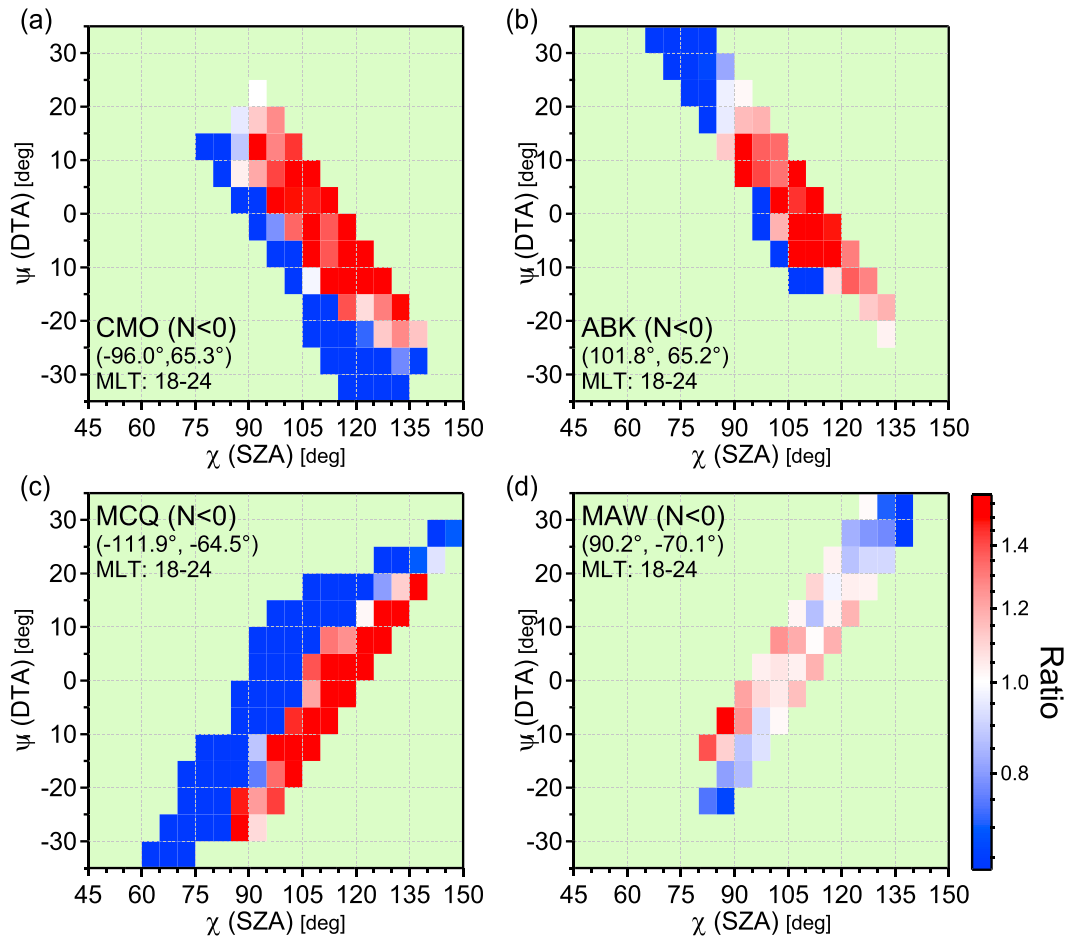


Figure 9. The DTA(ψ)-SZA(χ) diagrams of negative N at MLT = 18–24 for (a) CMO, (b) ABK, (c) MCQ, and (d) MAW for the southward (IMF $B_z \leq -1$ nT) condition. The median of N of each ψ - χ cell is normalized by its average over all cells in ψ - χ and shown in color.

by the red-to-blue pattern for all four stations. The reduction of N for large $|\psi|$ is suggestive for CMO (Figure 11a) and MAW (Figure 11d), but overall, it is not as clear as for negative N (Figures 9 and 10). The fact that the N magnitude is organized by DTA(ψ) versus SZA(χ) rather than by MLT versus SZA(χ) strongly suggests that although DTA(ψ) and SZA(χ) are correlated with each other, the DTA affects the N magnitude independently of the SZA.

Since the monoenergetic and broadband precipitation is most prevalent in the premidnight sector especially during substorms (e.g., Newell et al., 2010) and those two types of precipitation can be more intense in the dark hemisphere (section 4), we examined the WEJ and EEJ for MLT = 21–24, rather than MLT = 18–24 (Figures 9 and 11), in the same way. The DTA(ψ)-SZA(χ) diagram (not shown) basically confirms that the dark ionosphere is favorable for the WEJ but not for the EEJ; however, because the MLT range is only 3-hr wide, the SZA(χ) varies only within 10° , and accordingly, the SZA dependence turned out to be less clear. We also emphasize that the WEJ intensity is larger for larger χ not only in the dusk-to-midnight sector (Figure 9) but also in the midnight-to-dawn sector (Figure 10), and even in the dawn quadrant, MLT = 03–09 (not shown), where the WEJ is usually associated with the sunward return flow of the global two-cell convection. Therefore, although the monoenergetic and broadband precipitation may contribute to the preference for the dark hemisphere, it is probably not essential. Furthermore, the EEJ is more intense when the ionosphere is sunlit, which places an important constraint on the explanation of the solar illumination effect on the AEJs. That is, any explanation of the preference of the WEJ for the dark ionosphere has to also explain why it does not apply to the EEJ.

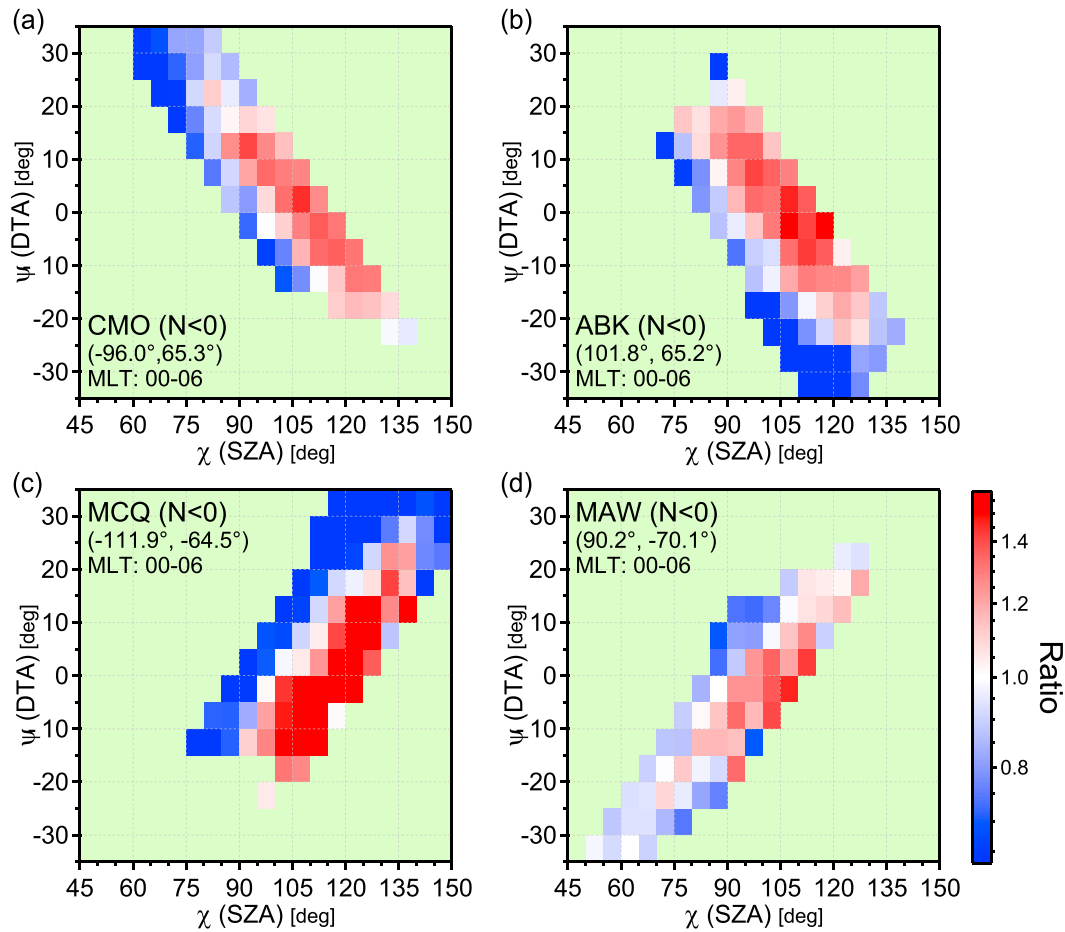


Figure 10. The DTA(ψ)-SZA(χ) diagrams of negative N at MLT = 00-06 for (a) CMO, (b) ABK, (c) MCQ, and (d) MAW for the southward (IMF $B_z \leq -1$ nT) condition.

4. Discussion

In the previous section we found for negative N^* that the SZA(χ) dependence, if organized by MLT, differs significantly among the four stations (Figure 7), but if additionally sorted by the DTA(ψ), the result, that is, the ψ - χ diagram, shows a consistent pattern (Figures 9 and 10). First we demonstrate that those various patterns of the MLT-SZA(χ) diagram can be reproduced from a simple ψ - χ dependence of the WEJ intensity as shown in Figure 12. In this figure we assume, based on the results of Figures 9 and 10, that the magnitude of N gets smaller with increasing $|\psi|$, and it increases with increasing χ . We emphasize that this ψ - χ diagram is for an explanation purpose only. The four curves represent the actual ψ - χ variations over a year (year = 2010) for the four stations that we examined, that is, CMO, ABK, MCQ, and MAW as denoted. The LT is fixed at LT = 04 and 22 for Figures 12a and 12b, respectively; for simplicity, we fixed LT, not MLT. In general, the DTA(ψ) and SZA(χ) are correlated negatively in Northern Hemisphere and positively in Southern Hemisphere. For a given LT, the corresponding UT is different for different stations and so is the DTA(ψ). Therefore, ψ has an offset, which depends on the coordinates of the station.

Figure 12 shows that N changes differently as a function of SZA(χ) along different ψ - χ curves. For LT = 04 (Figure 12a), as the SZA(χ) increases, the magnitude of N tends to increase for CMO, decrease for ABK, decrease for MCQ, and increase for MAW. Regarding MAW, since its curve is positioned relatively close to the middle of the DTA(ψ) range, N can actually have a peak in the middle of the corresponding χ range. These expectations are all consistent with the SZA(χ) dependence of N^* in the dawn sector (Figure 7). For LT = 22 (Figure 12b), as SZA(χ) increases, the magnitude of N tends to mostly decrease for CMO, increase for ABK, peak in the middle for MCQ, and decrease for MAW. Again, these expectations are all consistent

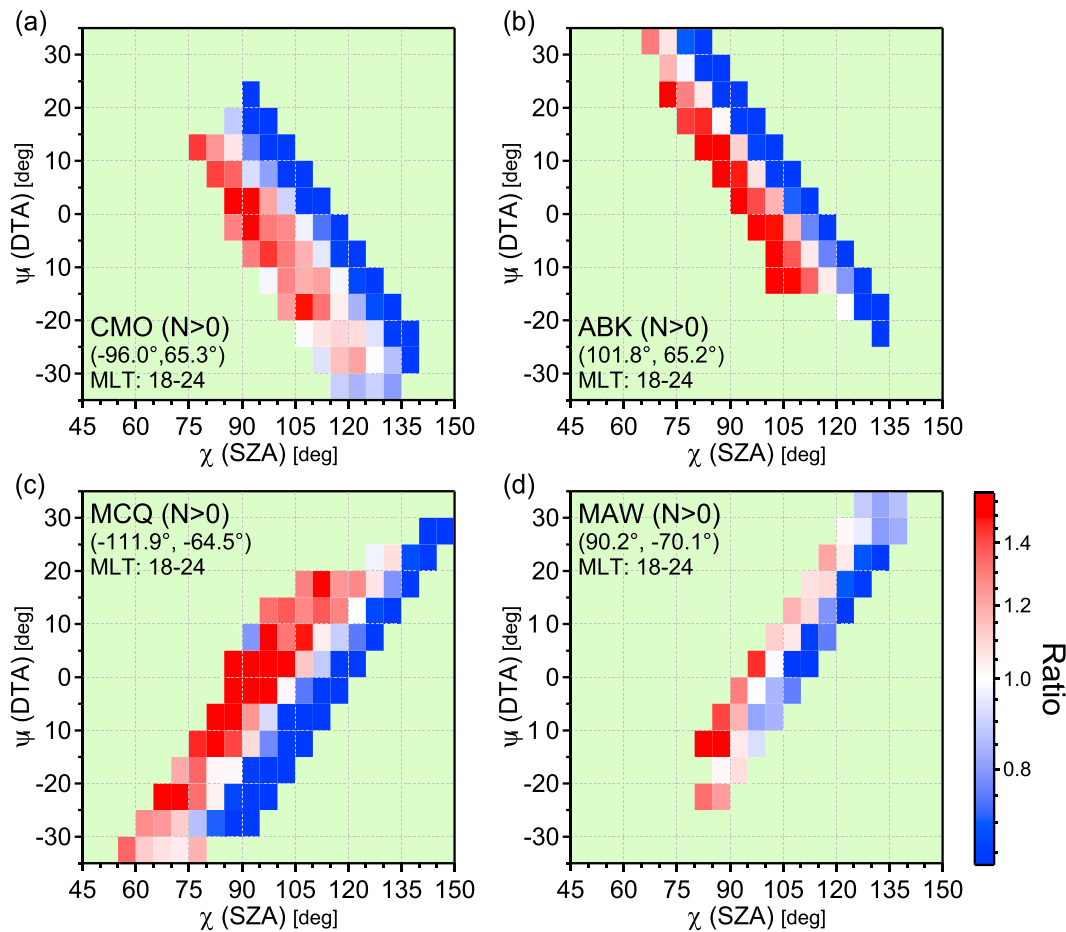


Figure 11. The DTA(ψ)-SZA(χ) diagrams of positive N at MLT = 18–24 for (a) CMO, (b) ABK, (c) MCQ, and (d) MAW for the southward (IMF $B_Z \leq -1$ nT) condition.

with the SZA(χ) dependence of N^* in Figure 7. The actual dependence of the WEJ on the DTA(ψ) and SZA(χ) may differ for different MLTs or for different drivers (i.e., global convection and substorms). Nevertheless, the versatility of this simple diagram in explaining the SZA(χ) dependence for different stations at different LTs suggests that it well reflects the underlying process of the DTA(ψ) and SZA(χ) dependence of the WEJ intensity.

The dependence of the solar wind (SW)-M-I coupling on the DTA(ψ) has been examined in terms of global geomagnetic indices such as AE and Dst , and it has been known that the coupling is more efficient when the dipole axis is less tilted either toward or away from Sun (e.g. Cliver et al., 2000, Svalgaard, 1977), which is often called the equinoctial effect. The efficiency of the SW-M-I coupling possibly reflects that of dayside reconnection, and indeed, a global modeling study suggested that the length of the dayside separatrix is shorter for a larger tilt angle (Cnossen et al., 2012), which results in a smaller cross-polar cap potential difference, and therefore, in lower geomagnetic activity. This result may be interpreted in terms of the deformation of the dayside magnetosphere by the R1 current, which likely affects the efficiency of the SW-M-I coupling (e.g. Merkin et al., 2003, Ohtani et al., 2014). Large dipole tilt is also unfavorable for the Kelvin-Helmholtz instability at the flanks of the magnetosphere since the magnetic field on the magnetospheric side tends to have a large component parallel to the magnetosheath flow, and the associated magnetic tension works against the instability (Boller & Stolov, 1970).

The dipole tilt effect on the SW-M-I coupling is not a focus of our study, which should be investigated with global measures of geomagnetic activity rather than with local geomagnetic disturbances. Nevertheless, our result strongly suggests that for the nightside AEJ intensity, the dipole tilt is as important as the solar

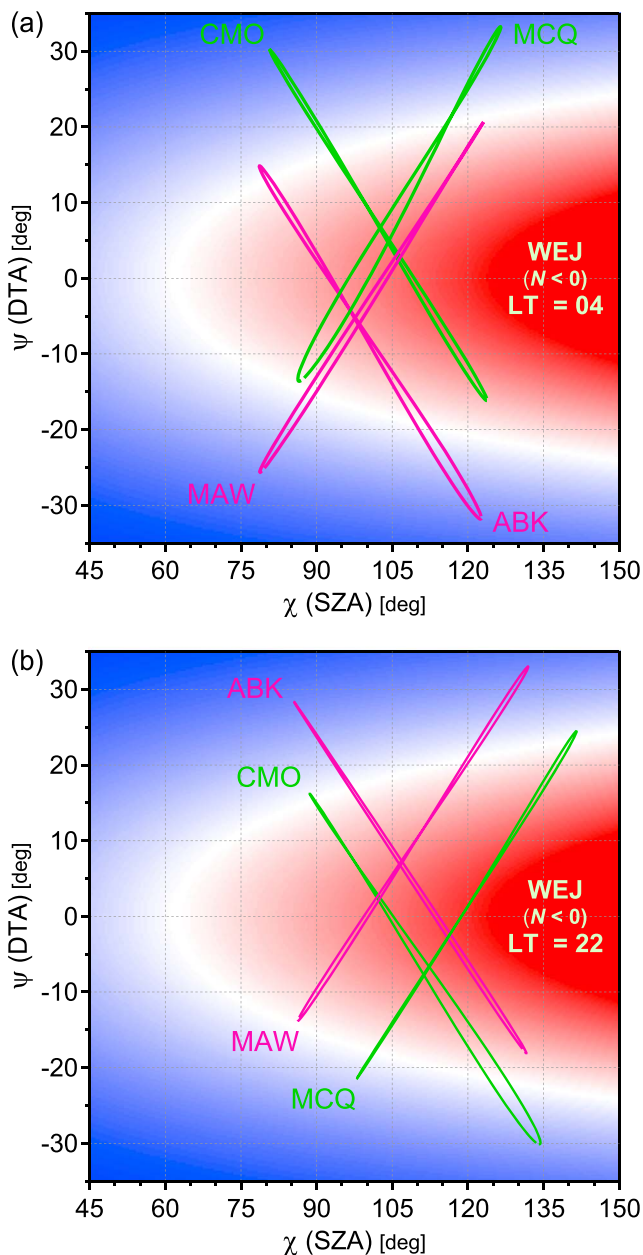


Figure 12. Schematic explanation of the variability of the SZA(χ) dependence of the negative N geomagnetic disturbance at different geomagnetic stations. The relative magnitude of the N disturbance is shown in the blue-to-red gradation in the DTA(ψ)-SZA(χ) frame (see text for details). The four curves show the actual ψ - χ variations at the four geomagnetic stations (i.e., CMO, ABK, MCQ, and MAW) at (a) LT = 04 and (b) LT = 22.

field-aligned potential difference is created to carry upward FACs imposed by the magnetosphere, and as a result, the auroral precipitation enhances the ionospheric conductance more in the dark hemisphere than in the sunlit hemisphere (Ohtani et al., 2009). Another idea concerns the feedback instability. This instability was proposed to explain the formation of discrete auroral arcs due to the phase matching between the advection of the ionospheric conductance modulation and the reflection of the Alfvén wave (e.g. Atkinson, 1970, Lysak, 1991, Sato, 1978). The associated electron precipitation modulates and enhances the ionospheric conductance more effectively if the background conductance is lower, and therefore, the dark ionosphere is favorable for the instability.

illumination. Since the AEJ is physically linked with other quantities such as FACs and auroral precipitation, the effects of the dipole tilt and solar illumination are probably comparable for the nightside M-I system, in general. This point is also critical for addressing the seasonal dependence of geomagnetic activity.

In the rest of this discussion, we focus on the difference in the solar illumination dependence between the WEJ and EEJ, more specifically, the possible reason why the WEJ tends to be more intense when the ionosphere is dark (Figures 9 and 10), whereas the EEJ tends to be more intense when the ionosphere is sunlit (Figure 11).

First we note that for this issue the solar illumination dependence of the ionospheric electric field, if any, is not essential. We can address this point in terms of the asymmetry between the sunlit and dark hemispheres since we are concerned mostly with the nightside AEJs; if the AEJ is sunlit in one hemisphere, it is dark at the conjugate point. Here any interhemispheric difference of the ionospheric electric field can be attributed to that of the field-aligned potential difference. However, the occurrence of monoenergetic auroral precipitation, which is a manifestation of the field-aligned potential difference, is distributed mostly in the dusk-to-midnight sector, where the EEJ, rather than the WEJ, prevails except at premidnight (Figure 1). Moreover, the field-aligned potential difference is generally much smaller than the cross-magnetic field potential difference, and it tends to be larger in the dark hemisphere than in the sunlit hemisphere (Newell et al., 1996, 2010), which suggests that the ionospheric electric field, if it is different between the two hemispheres, is smaller in the dark hemisphere. Therefore, whereas this may contribute to the preference of the EEJ for the sunlit hemisphere, it does not explain why the WEJ tends to be more intense in the dark hemisphere.

We therefore focus on the ionospheric conductance. The result of our study strongly suggests that for the WEJ, the ionospheric conductance tends to be higher when the ionosphere is dark than when it is sunlit, but the other way around for the EEJ. Obviously, the key is auroral precipitation. Interestingly, Gjerloev et al. (2010) found that during the growth phase of isolated substorms, for which auroral precipitation is generally at low levels, not only the EEJ but also the WEJ is more intense in the sunlit hemisphere than in the dark hemisphere. We therefore infer from the results of our study and Gjerloev et al.'s that for the WEJ, once geomagnetic activity enhances, the auroral precipitation intensifies more in the dark hemisphere than in the sunlit hemisphere.

There are two possible ideas suggested in the past for explaining more intense M-I coupling in the dark hemisphere than in the sunlit hemisphere. One is based on the interhemispheric asymmetry of the plasma density in the auroral acceleration region, which is lower in the winter/dark hemisphere (Johnson et al., 2001). Accordingly, a larger

The relevant electron precipitation, whether monoenergetic or broadband, is prevalent in the dusk-to-midnight sector and more intense in winter than in summer (Newell et al., 2010). Therefore, those ideas may explain why in the premidnight sector the WEJ is more intense when the ionosphere is dark. However, it does not explain why the EEJ does not reveal a similar preference in the same MLT sector. More critically, the energy flux of those two types of electron precipitation is much lower in the midnight-to-dawn sector (e.g., Newell et al., 2009), where the WEJ becomes more intense when the ionosphere is dark (Figure 10). Therefore, our results strongly suggest that there is another process that prevails in the midnight-to-dawn sector and works preferentially in the dark hemisphere.

The diffuse auroral precipitation is the most plausible candidate for this missing process. The diffuse precipitation takes place in a wide range of MLT extending from premidnight to late morning, and it constitutes the majority of auroral energy deposition to the ionosphere (Newell et al., 2009). Therefore, it is the primary source of the ionospheric conductance in the corresponding sector. Furthermore, the energy flux of diffuse aurora is higher in the winter/dark hemisphere than in the summer/sunlit hemisphere (Hamrin et al., 2005; Newell et al., 2010). These features are consistent with the preference of the WEJ for the dark ionosphere (Figures 9 and 10). This idea, however, still does not explain why the EEJ in the evening-to-midnight sector is more intense when the ionosphere is sunlit rather than when it is dark (Figure 11). One speculative idea is that when the AEJ is directed eastward in the premidnight sector, as opposed to westward as expected for substorm periods, the geomagnetic activity tends to be lower and accordingly, the observation of the EEJ itself is biased to weaker auroral precipitation. In fact, Figure 1 shows that although the number of the 5-min data points is comparable for positive and negative N (Figure 1), its magnitude is significantly smaller for positive N than for negative N . Accordingly, the solar illumination is considered to play a more important role for positive N than for negative N .

Therefore, for understanding the solar illumination dependence of the M-I current system, it is critical to understand that of the diffuse electron precipitation. However, the conventional explanation of the diffuse precipitation attributes it to the pitch angle scattering of plasma sheet electrons into the loss cones (e.g., Ni et al., 2016), for which we usually do not expect any interhemispheric asymmetry.

One interesting clue is that the interhemispheric asymmetry of the diffuse electron precipitation is more significant for the energy flux than for the number flux (Newell et al., 2010), which suggests that its average energy is higher in the dark hemisphere than in the sunlit hemisphere. There are two possibilities for this. One is that more energetic electrons are scattered into the loss cone to the dark hemisphere, which requires that the generation or propagation of responsible waves (e.g., chorus and electrostatic electron cyclotron harmonic waves) is not symmetric with respect to the equator. Another possibility is that the electrons are accelerated on their way to the ionosphere. The diffuse precipitation is usually identified as a type of precipitation that cannot be classified as either monoenergetic or broadband. Therefore, if electrons are accelerated by a field-aligned potential difference, which, however, is smaller than the electron thermal energy, their precipitation can be identified as diffuse rather than monoenergetic. Then the preference of the diffuse precipitation for the dark hemisphere may be explained in the same way as that of monoenergetic precipitation.

The generation of secondary electrons, which can be an important component of the diffuse precipitation (Khazanov et al., 2017), may also contribute to its interhemispheric asymmetry. If more secondary electrons are produced in the sunlit nightside hemisphere, possibly because of a largescale height, they would contribute to the enhancement of the diffuse precipitation in the dark hemisphere. Note, however, that this process itself does not include any acceleration.

Obviously, these ideas need to be examined more closely in the future, and we hope that the present study will draw more attention to the interhemispheric asymmetry of the diffuse precipitation, which, as suggested by this study, is a key to understanding the interhemispheric asymmetry of the M-I system even though it has been widely overlooked.

5. Summary

In the present study we investigated the dependence of the local AEJ intensity on the solar illumination. We used negative and positive N component (northward) magnetic disturbances as measures of the WEJ and EEJ intensities, respectively, and the SZA(χ) as a measure of the local solar illumination. First we

examined the N magnitude at ABK in the MLT-SZA(χ) frame, and we found that on the dayside, both WEJ and EEJ are more intense when the ionosphere is sunlit, which can be attributed to the enhanced ionospheric conductance by the solar EUV irradiance. On the nightside, in contrast, the AEJ intensity depends on SZA(χ) in a more complex way. Most noticeably, the intensity of the WEJ in the premidnight sector is more intense when the ionosphere is dark than when it is sunlit. Whereas other stations in the same sector reveal similar MLT-SZA(χ) patterns, the pattern for negative N differs significantly among stations at different longitudes and in different hemispheres. However, such variability disappears if we additionally sort data by the DTA(ψ), which suggests that the dipole tilt is an independent factor that controls the AEJ intensity, and its effect on the local AEJ intensity is comparable to that of the SZA. We found that the AEJ is more intense when the dipole is less tilted either toward or away from Sun (i.e., for smaller $|\psi|$), which is consistent with the result of the past studies of the dipole tilt effect. Most importantly, the preference of the nightside WEJ for the dark ionosphere, as we reconfirmed with the DTA(ψ)-SZA(χ) diagram, is not limited to the pre-midnight sector, but it extends from premidnight to dawn suggesting that this preference is a feature for the WEJ in general, and it does not matter whether it is driven by substorms or by global convection. In contrast, we found that the EEJ is more intense in the sunlit hemisphere. This difference between the WEJ and EEJ is difficult to explain in terms of the previously proposed ideas of the preference of the monoenergetic or broadband precipitation for the dark ionosphere. Instead, the MLT distribution and solar illumination dependence of the WEJ are similar to those of the diffuse auroral precipitation. It is therefore suggested that the observed preference of the WEJ for the dark ionosphere reflects the interhemispheric asymmetry of ionospheric conductance due to the diffuse auroral precipitation.

Acknowledgments

We thank the United States Geological Survey (USGS) for the College (CMO) ground magnetometer data. We also thank Sodankylä Geophysical Observatory of the University of Oulu for the Sodankylä (SOD) ground magnetometer data. The ground magnetometer data that we used in this study, including the CMO and SOD data, were provided through the SuperMAG website (<http://supermag.jhuapl.edu/>). SuperMAG is an international collaboration with many organizations and institutes funded by National Science Foundation (NSF). The OMNI data were provided by the GSFC/SPDF OMNIWeb at <https://omniweb.gsfc.nasa.gov>. Support for this analysis at the Johns Hopkins University Applied Physics Laboratory was provided by National Aeronautics and Space Administration (NASA) Grant NNX16AG74G and National Science Foundation (NSF) Grants 1502700 for S. O. and 1417899 for J. W. G.

References

- Akasofu, S.-I., Chapman, S., & Meng, C.-I. (1965). The polar electrojet. *Journal of Atmospheric and Terrestrial Physics*, 27, 1279.
- Atkinson, G. (1970). Auroral arcs: Result of the interaction of a dynamic magnetosphere with the ionosphere. *Journal of Geophysical Research*, 75(25), 4746–4755. <https://doi.org/10.1029/JA075i025p04746>
- Boller, B. R., & Stolo, H. L. (1970). Kelvin-Helmholtz instability and the semiannual variation of geomagnetic activity. *Journal of Geophysical Research*, 75(31), 6073–6084. <https://doi.org/10.1029/JA075i031p06073>
- Cliver, E. W., Kamide, Y., & Ling, A. G. (2000). Mountains versus valleys: Semiannual variation of geomagnetic activity. *Journal of Geophysical Research*, 105(A2), 2413–2424. <https://doi.org/10.1029/1999JA900439>
- Cnossen, I., Wiltberger, M., & Ouellette, J. E. (2012). The effects of seasonal and diurnal variations in the Earth's magnetic dipole orientation on solar wind-magnetosphere-ionosphere coupling. *Journal of Geophysical Research*, 117, A11211. <https://doi.org/10.1029/2012JA017825>
- Coxon, J. C., Milan, S. E., Carter, J. A., Clausen, L. B. N., Anderson, B. J., & Korth, H. (2016). Seasonal and diurnal variations in AMPERE observations of the Birkeland currents compared to modeled results. *Journal of Geophysical Research: Space Physics*, 121, 4027–4040. <https://doi.org/10.1002/2015JA022050>
- Fujii, R., Potemra, T. A., & Sugiura, M. (1981). Seasonal dependence of large-scale Birkeland current intensities under geomagnetic quiet conditions. *Geophysical Research Letters*, 8(10), 1103–1106. <https://doi.org/10.1029/GL008i010p01103>
- Gjerloev, J. W. (2012). The SuperMAG data processing technique. *Journal of Geophysical Research*, 117, A09213. <https://doi.org/10.1029/2012JA017683>
- Gjerloev, J. W., Hoffman, R. A., Ohtani, S., Weygand, J., & Barnes, R. (2010). Response of the auroral electrojet indices to abrupt southward IMF turnings. *Annales Geophysicae*, 28(5), 1167–1182. <https://doi.org/10.5194/angeo-28-1167-2010>
- Hamrin, M., Norqvist, P., Rönmark, K., & Fellgard, R. (2005). The importance of solar illumination for discrete and diffuse aurora. *Annales Geophysicae*, 23(11), 3481–3486. <https://doi.org/10.5194/angeo-23-3481-2005>
- Haraguchi, K., Kawano, H., Yumoto, K., Ohtani, S., Higuchi, T., & Ueno, G. (2004). Ionospheric conductivity dependence of dayside region-0, 1, and 2 field-aligned current systems: Statistical study with DMSP-F7. *Annales Geophysicae*, 22(8), 2775–2783. <https://doi.org/10.5194/angeo-22-2775-2004>
- Heppner, J. P., & Maynard, N. C. (1987). Empirical high-latitude electric field models. *Journal of Geophysical Research*, 92(A5), 4467–4489. <https://doi.org/10.1029/JA092iA05p04467>
- Johnson, M. T., Wygant, J. R., Cattell, C., Mozer, F. S., Temerin, M., & Scudder, J. (2001). Observations of the seasonal dependence of the thermal plasma density in the Southern Hemisphere auroral zone and polar cap at 1 RE. *Journal of Geophysical Research*, 106(A9), 19,023–19,033. <https://doi.org/10.1029/2000JA900147>
- Khazanov, G. V., Sibeck, D. G., & Zesta, E. (2017). Is diffuse aurora driven from above or below? *Geophysical Research Letters*, 44, 641–647. <https://doi.org/10.1002/2016GL072063>
- Laundal, K. M., & Gjerloev, J. W. (2014). What is the appropriate coordinate system for magnetometer data when analyzing ionospheric currents? *Journal of Geophysical Research: Space Physics*, 119, 8637–8647. <https://doi.org/10.1002/2014JA020484>
- Lin, C. S., & Hoffman, R. A. (1979). Characteristics of the inverted-V event. *Journal of Geophysical Research*, 84(A4), 1514–1524. <https://doi.org/10.1029/JA084iA04p01514>
- Liou, K., Newell, P. T., & Meng, C. I. (2001). Seasonal effects on auroral particle acceleration and precipitation. *Journal of Geophysical Research*, 106(A4), 5531–5542. <https://doi.org/10.1029/1999JA000391>
- Lui, A. T. Y., Akasofu, S.-I., Hones, E. W. Jr., Bame, S. J., & McIlwain, C. E. (1976). Observation of the plasma sheet during a contracted oval substorm in a prolonged quiet period. *Journal of Geophysical Research*, 81(7), 1415–1419. <https://doi.org/10.1029/JA081i007p01415>
- Lysak, R. L. (1991). Feedback instability of the ionospheric resonant cavity. *Journal of Geophysical Research*, 96(A2), 1553–1568. <https://doi.org/10.1029/90JA02154>

- Merkin, V. G., Papadopoulos, K., Milikh, G., Sharma, A. S., Shao, X., Lyon, J., & Goodrich, C. (2003). Effects of the solar wind electric field and ionospheric conductance on the cross polar cap potential: Results of global MHD modeling. *Geophysical Research Letters*, 30(23), 2180. <https://doi.org/10.1029/2003GL017903>
- Newell, P. T., Meng, C.-I., & Lyons, K. M. (1996). Discrete aurorae are suppressed in sunlight. *Nature*, 381(6585), 766–767. <https://doi.org/10.1038/381766a0>
- Newell, P. T., Sotirelis, T., & Wing, S. (2009). Diffuse, monoenergetic, and broadband aurora: The global precipitation budget. *Journal of Geophysical Research*, 114, A09207. <https://doi.org/10.1029/2009JA014326>
- Newell, P. T., Sotirelis, T., & Wing, S. (2010). Seasonal variations in diffuse, monoenergetic, and broadband aurora. *Journal of Geophysical Research*, 115, A03216. <https://doi.org/10.1029/2009JA014805>
- Ni, B., Thorne, R. M., Zhang, X., Bortnik, J., Pu, Z., Xie, L., et al. (2016). Origins of the Earth's diffuse auroral precipitation. *Space Science Reviews*, 200(1-4), 205–259. <https://doi.org/10.1007/s11214-016-0234-7>
- Nishida, A. (1968). Geomagnetic D_p 2 fluctuations and associated magnetospheric phenomena. *Journal of Geophysical Research*, 73(5), 1795–1803. <https://doi.org/10.1029/JA073i005p01795>
- Ohtani, S., Ueno, G., & Higuchi, T. (2005). Comparison of large-scale field-aligned currents under sunlit and dark ionospheric conditions. *Journal of Geophysical Research*, 110, A09230. <https://doi.org/10.1029/2005JA011057>
- Ohtani, S., Ueno, G., Higuchi, T., & Kawano, H. (2005). Annual and semiannual variations of the location and intensity of large-scale field-aligned currents. *Journal of Geophysical Research*, 110, A01216. <https://doi.org/10.1029/2004JA010634>
- Ohtani, S., Wing, S., Merkin, V. G., & Higuchi, T. (2014). Solar cycle dependence of nightside field-aligned currents: Effects of dayside ionospheric conductivity on the solar wind-magnetosphere-ionosphere coupling. *Journal of Geophysical Research: Space Physics*, 119, 322–334. <https://doi.org/10.1002/2013JA019410>
- Ohtani, S., Wing, S., Ueno, G., & Higuchi, T. (2009). Dependence of premidnight field-aligned currents and particle precipitation on solar illumination. *Journal of Geophysical Research*, 114, A12205. <https://doi.org/10.1029/2009JA014115>
- Sato, T. (1978). A theory of quiet auroral arcs. *Journal of Geophysical Research*, 83(A3), 1042. <https://doi.org/10.1029/JA083iA03p01042>
- Svalgaard, L. (1977). Geomagnetic activity: Dependence on solar wind parameters. In J. B. Zirker (Ed.), *Skylab Workshop on Coronal Holes* (pp. 371–441). Boulder, CO: Colorado Association University Press.
- Wang, H., Lühr, H., & Ma, S. Y. (2005). Solar zenith angle and merging electric field control of field-aligned currents: A statistical study of the Southern Hemisphere. *Journal of Geophysical Research*, 110, A03306. <https://doi.org/10.1029/2004JA010530>